Water Resources Research

Lithologically Controlled Subsurface Critical Zone Thickness and Water Storage Capacity Determine Regional Plant Community Composition

W. Jesse Hahm[1], Daniella M. Rempe[2], David N. Dralle[1], Todd E. Dawson[3], Sky M. Lovill[1], Alexander B. Bryk[1], David L. Bish[4], Juergen Schieber[4], and William E. Dietrich[1]

[1]Department of Earth and Planetary Science, University of California, Berkeley, CA, USA, [2]Jackson School of Geosciences, Department of Geological Science, University of Texas at Austin, Austin, TX, USA, [3]Center for Stable Isotope Biogeochemistry, Department of Integrative Biology, University of California, Berkeley, CA, USA, [4]Department of Earth and Atmospheric Sciences, Indiana University, Bloomington, IN, USA

Abstract Explanations for distinct adjacent ecosystems that extend across hilly landscapes typically point to differences in climate or land use. Here we document—within a similar climate—how contrasting regional plant communities correlate with distinct underlying lithology and reveal how differences in water storage capacity in the critical zone (CZ) explain this relationship. We present observations of subsurface CZ structure and groundwater dynamics from deep boreholes and quantify catchment-wide dynamic water storage in two Franciscan rock types of the Northern California Coast Ranges. Our field sites have a Mediterranean climate, where rains are out of phase with solar energy, amplifying the importance of subsurface water storage for periods of peak ecosystem productivity in the dry season. In the deeply weathered (~30 m at ridge) Coastal Belt argillite and sandstone, ample, seasonally replenished rock moisture supports an evergreen forest and groundwater drainage sustains baseflow throughout the summer. In the Central Belt argillite-matrix mélange, a thin CZ (~3 m at ridge) limits total dynamic water storage capacity (100–200 mm) and rapidly sheds winter rainfall via shallow storm and saturation overland flow, resulting in low plant-available water (inferred from predawn tree water potential) and negligible groundwater storage that can drain to streams in summer. This storage limitation mechanism explains the presence of an oak savanna-woodland bounded by seasonally ephemeral streams, despite >1,800 mm of average precipitation. Through hydrologic monitoring and subsurface characterization, we reveal a mechanism by which differences in rock type result in distinct regionally extensive plant communities under a similar climate.

Plain Language Summary The ability of the subsurface critical zone—extending from the ground surface down to fresh, unweathered bedrock—to store and release water to plants and streams is a key variable explaining ecosystem composition and function. The storage and release of water are particularly important in Mediterranean climates, where rain arrives in winter and summers are typically warm and dry. Here plants rely half the year on seasonally replenished water from belowground. We documented how the subsurface structure of the critical zone determines how water is shed from landscapes and how much water can be seasonally stored. We found that locations with a thicker critical zone had higher water storage capacity, more productive ecosystems, deeper groundwater runoff generation, and greater summer streamflow. Where the critical zone is thin and storage capacity is limited, the subsurface completely saturates, and the landscape sheds incoming rain via surface runoff. This water storage limitation explains the presence of an oak savanna-woodland in the Northern California Coast Ranges, where rainfall is ample, and neighboring areas experiencing similar climate have towering forest canopies. Rock type governed these variations, highlighting its importance in determining the distribution of ecosystems and water runoff pathways to streams.

1. Introduction

Large-scale variations in the vegetation composition across landscapes are commonly explained by climatic gradients, which exert a primary control on water and energy availability (Holdridge, 1947; Stephenson, 1990; Whittaker, 1975). However, within any particular climate, distinct plant communities may coexist, unexplained by regional temperature or precipitation. These vegetation mosaics may result from patterns

of anthropogenic land use but can also arise from a variety of ecosystem processes, including herbivory, clustering, dispersal-limitation, or disturbance-induced succession (Aguiar & Sala, 1994; Bond, 2005; Dantas et al., 2016; Heinselman, 1981; Polis, 1999; Scanlon et al., 2007). Variations in microclimate, such as those arising from hillslope aspect (Holland & Steyn, 1975; Parker, 1982), or contrasting underlying lithology, which can influence toxin or nutrient delivery to plants (Hahm et al., 2014; Kruckeberg, 2004), can similarly demarcate abrupt vegetation boundaries.

In water-limited environments, soil water storage capacity can influence plant-available water and the onset of plant water stress, impacting primary productivity and plant water use (Barkaoui et al., 2017; Branson et al., 1970; Laio et al., 2001; Porporato et al., 2001, 2004; Prentice et al., 1992; Smith et al., 1995). Even in climates with ample precipitation, storage limitations belowground can result in water limitation, affecting the distribution of plants (Rodriguez-Iturbe et al., 2007). This is likely common in Mediterranean climates, where the delivery of precipitation is out of phase with solar energy availability and atmospheric moisture demand. In these regions, the importance of the subsurface is amplified, due to its role in storing rainfall that falls in the wet season and releasing that water to ecosystems in summer.

Plants in upland landscapes with thin soils may survive on water extracted from the weathered bedrock from below the soil, exploiting either groundwater (e.g., Miller et al., 2010) or rock moisture (sensu Salve et al., 2012; Rempe & Dietrich, 2018) from tens of meters below the ground surface (e.g., Anderson et al., 1995; Arkley, 1981; Bales et al., 2011; Eliades et al., 2018; Jones & Graham, 1993; Lewis & Burgy, 1964; Miller et al., 2010; Rempe & Dietrich, 2018; Rose et al., 2003; Sternberg et al., 1996; Zunzunegui et al., 2018; Zwieniecki & Newton, 1996). These and other previous studies in seasonally dry environments, however, have focused on local, site-specific plant water use and have not explicitly addressed larger-scale relationships between dominant vegetation patterns and the spatial availability of moisture beneath the soil.

Research in critical zone science now suggests that there may be predictable, lithologically controlled regional patterns of weathered bedrock thickness across landscapes (Riebe et al., 2017). The depth and extent of weathering and the associated porosity increase must control the potential for moisture storage (e.g., Klos et al., 2018), which, in turn, should affect the composition of aboveground plant community assemblages, especially in seasonally dry environments. This leads to the hypothesis that bedrock weathering patterns and associated water storage capacity should have a profound—yet hitherto undocumented—effect on regional patterns of plant water use, productivity, and species distribution in seasonally dry climates. This emerging view has not yet been tested. It presents a challenge because the extent of bedrock weathering is difficult to measure (typically requiring drilling or geophysics), and therefore difficult to document at large spatial scales.

Here we explore whether differences in subsurface critical zone development associated with differences in lithology can provide an explanation for a dramatic regional-scale contrast in dominant vegetation assemblage that extends for over 200 km (Figures 1–3). Our study region is located along the unglaciated Northern California Coast Ranges, where adjacent landscapes, underlain by different lithologic units of the Franciscan Formation complex support strikingly different plant communities. To the west, a towering evergreen forest mantles the steep hillslopes of the Coastal Belt, comprised of turbidite sequences of argillite, sandstone, and minor conglomerate. Sharply juxtaposed to the east are the rolling hills of the Central Belt, which is a mélange of geochemically similar yet metamorphosed and pervasively deformed Coastal Belt material. In the Central Belt mélange, the vegetation is a sparse deciduous-oak annual-grass savanna-woodland (Figures 1–3). These differences in plant communities occur despite the fact that both landscapes experience essentially the same annual rainfall (>1,800 mm) and mean annual temperature (about 13 °C). As Figure 4 shows, 1,800 mm greatly exceeds the expected precipitation range of a grassland savanna. Simply put, why would grassland savanna be the dominant vegetation in such a wet environment?

To test the hypothesis that the subsurface critical zone water storage capacity controls regional-scale vegetation distribution, we combine an analysis of regional-scale geologic maps, remotely sensed land cover and plant characteristics with a field-based "unit hillslope" approach at individual, intensively monitored sites. Landscapes are a collection of hillslopes bordered by channels that collect and drain watersheds. Rather than attempt to characterize the critical zone properties over a large area (which is presently very difficult to do), we focus on intensive measurements of properties and processes on what we estimate to be a representative (unit) hillslope within a given lithology. We assume that the commonality of topographic form
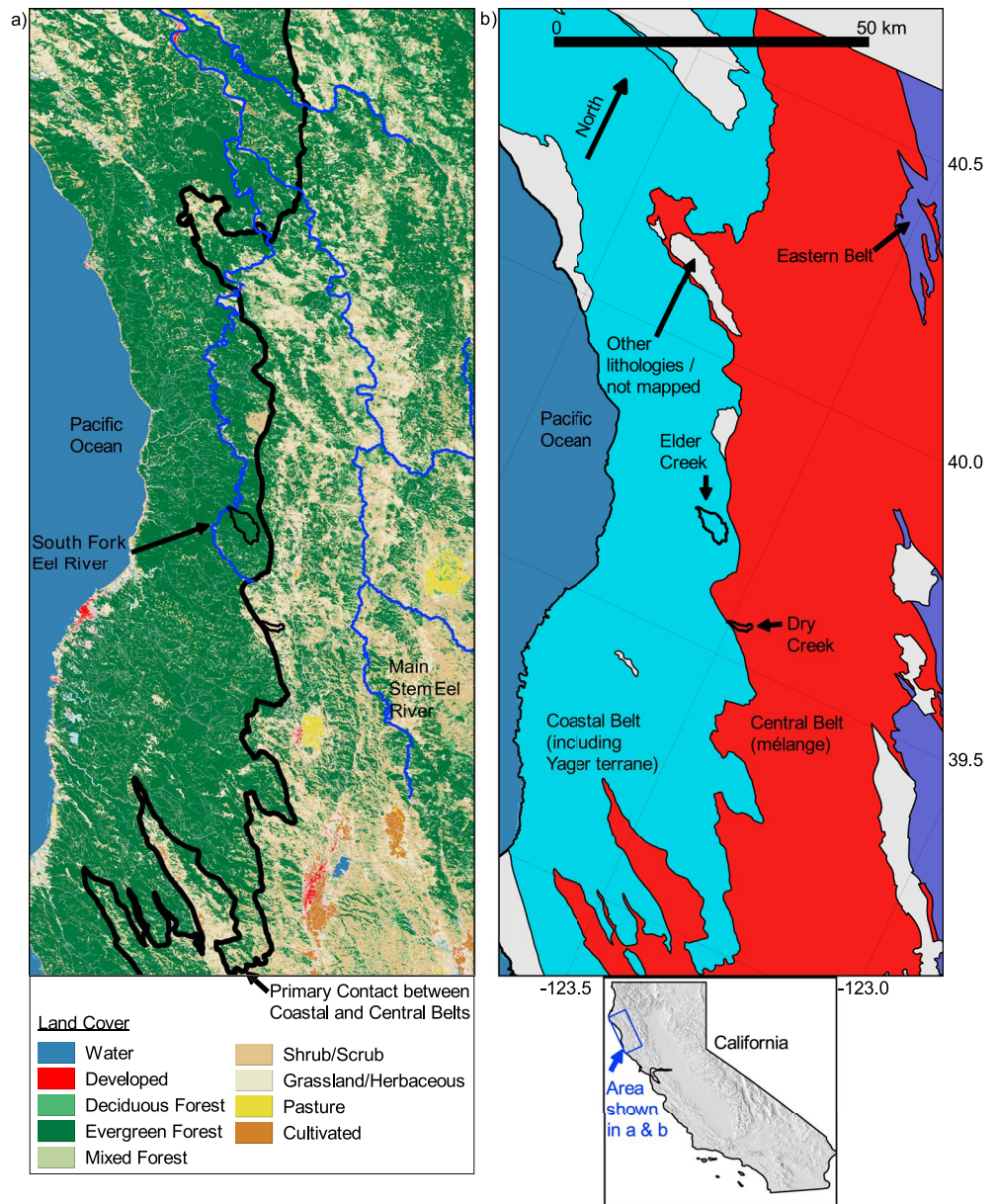
Figure 1. Comparison of land cover (a; 2011 National Land Cover Database [Homer et al., 2015]) and Franciscan bedrock geology (b; Langenheim et al., 2013). Blue lines in (a) show primary forks of the Eel River. Map inspired by Figure 2 of Lovill et al. (2018).

between repeating adjacent hillslopes reflects a commonality in the underlying weathering zone structure. This is consistent with current theories for critical zone evolution that propose that subsurface properties vary systematically with hillslope topography and lithology (Riebe et al., 2017). We then use the mechanistic understanding gained at the unit hillslope scale to interpret and explain watershed and regional-scale runoff, water budgets, and plant community assemblage dependence on critical zone properties.

Prior studies have generated extensive documentation of a unit hillslope ("Rivendell") in the forested-dominated Coastal Belt (Kim et al., 2014; Link et al., 2014; Oshun et al., 2016; Rempe & Dietrich, 2014, 2018; Salve et al., 2012). We initiated a new unit hillslope study in the Central Belt by exploring the subsurface with deep boreholes, establishing a network of monitoring wells, and monitoring weather and stream runoff. Here we report the results of this study, as well as new data for both sites on end-of-summer
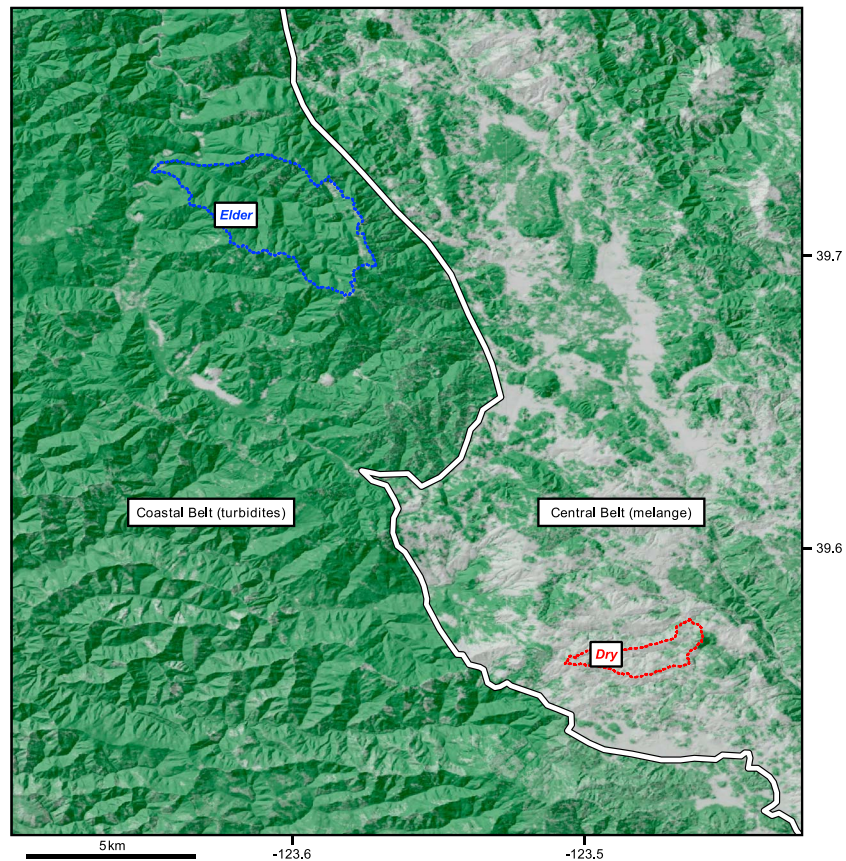
Figure 2. Tree canopy cover map of the field area shows the abrupt change in tree canopy cover at the geologic contact (white bold line) that separates the Coastal Belt (west) from the Central Belt (east) in the study area. Green (forested) patches in mélange are primarily on sandstone blocks. Study watersheds in each rock type are demarcated with dashed lines; gray = 0% canopy cover, darkest green = 100% canopy cover. Coordinates in WGS84; geologic contact after Jayko et al., 1989. Canopy cover from the 2011 National Land Cover Database. Map inspired by Figure 2 of Dralle et al. (2018).

predawn tree water potentials, composite annual time series of remotely sensed vegetation indices, bulk mineralogy and geochemistry, and tree canopy cover. For the Central Belt site, we also report new cosmogenic nuclide-based erosion rates, dissolved oxygen concentrations in groundwater, scanning electron microscopy imagery of fresh bedrock, and historical air photo analysis.

2. Site Description

2.1. Location and History

The two field sites, Angelo Coast Range Reserve ("Angelo," in the Coastal Belt) and the Sagehorn-Russell Ranch ("Sagehorn," in the Central Belt) form the core of the intensive monitoring sites in the Eel River Critical Zone Observatory. Angelo is part of the University of California Natural Reserve System and consists largely of steep-sloped, old-growth mixed broadleaf-needleleaf evergreen forest (see map in supporting information Figure S1). It contains the Elder Creek watershed (Table 1), a tributary to the South Fork Eel River, and Rivendell, an intensively instrumented hillslope that has been the site of numerous isotopic, geochemical, ecophysiological, and hydrologic studies (Dralle et al., 2018; Druhan et al., 2017; Kim et al., 2014, 2017; Link et al., 2014; Lovill et al., 2018; Oshun et al., 2016; Rempe & Dietrich, 2018; Salve et al., 2012; Simonin et al., 2014). Rivendell (39.729°, −123.6451°) is ~15 km east of the Pacific Ocean, 430 m above sea level (a.s.l.).

Sagehorn, a privately owned ranch, contains the Dry Creek watershed (Table 1; see map in supporting information Figure S2), which is in the main stem Eel River watershed. The site is dominated by a deciduous oak savanna-woodland, with predominantly nonnative annual herbaceous ground cover. There are dispersed

Figure 3. (a) Photo from headwaters of Elder Creek in the Coastal Belt, looking west, shows mixed broadleaf-needleleaf evergreen forest grading to chaparral on higher elevation, south-facing steep slopes. (b) Photo from northern ridge of Dry Creek watershed, looking north, shows annual-grass dominated, low-gradient hillslopes, with leafless winter-deciduous mistletoe-infested *Q. garryana* in foreground. The lumpy topography records relict earthflows. (c) Photo of south-facing tributary of Dry Creek during rainstorm (10 January 2017), showing extent of wetted channels and widespread saturation overland flow. Person for scale (170 cm tall); point in lower-right drains area of approximately 2 ha. (d) Panoramic photo between wells 503 and 500 at the Sagehorn Central Belt site along ridgetop on northern boundary of the Dry Creek catchment, showing complete saturation of the subsurface and overland flow in a winter rainstorm (190-cm-tall person in yellow jacket for scale).

densely forested areas that more closely resemble the vegetation community of Angelo that are situated primarily on sandstone blocks within the mélange. The principal study hillslope (39.5678°, −123.4733°) lies along an east-west running ridge on the northern border of the east-flowing Dry Creek, ~25 km east of the Pacific Ocean and 700 m above sea level.

2.2. Climate

The field areas experience a Mediterranean climate, with warm, dry summers and wet (rain-dominated), cool winters. Although both sites are near the coast, fog blankets the Dry Creek catchment at Sagehorn in the Central Belt only a few days a year and rarely enters the Elder Creek catchment in the Coastal Belt due to strong topographic barriers. Historical climate data (summarized in Table 2) indicate that Angelo (in the Coastal Belt) received ~2,000 mm of annual precipitation on average over the past century, 10–30% more than Sagehorn (in the Central Belt), and is slightly (~1 °C) cooler. However, due to greater interception losses at Angelo (see discussion below and analysis by Dralle et al., 2018), the amount of rainfall arriving at the ground surface is nearly identical at both sites. Both sites experience high interannual precipitation variability resulting in periodic drought conditions (Dettinger et al. (2011) report that the regional coefficient of variation of annual water year precipitation between 1951 and 2008 was 0.3 to 0.4).

2.3. Geology

This area of the Northern California Coast Ranges is primarily underlain by the Franciscan Formation complex (Table 3), which is divided into three generally north-south (coast-parallel) trending belts that are separated by fault contacts and decrease in age, subduction depth, and metamorphic grade to the west (Blake, 1974; Blake et al., 1985; Irwin, 1960; McLaughlin et al., 1994). The Coastal and Central Belts underlie ~15% and ~50% of the Eel River watershed, respectively (Langenheim et al., 2013). The Elder Creek watershed and our intensively studied hillslope, Rivendell, are underlain by Coastal Belt turbidites (which we group together with the lithologically similar and sometimes subdivided Yager terrane) and primarily consist of argillite with smaller amounts of interbedded sandstone (greywacke) and minor conglomerate (Jayko et al., 1989; Lovill et al., 2018).

Sagehorn is underlain by the Central Belt, which is locally interpreted to be a low-temperature, high-pressure tectonic flow mélange (Cloos, 1982). The mélange matrix is primarily argillaceous (mudstone protolith) and has a scaly appearance (Blake, 1974). The matrix grades over distances of tens of meters from fractured and folded but bedded mudstone into argillaceous material exhibiting "anastamosing fracture cleavage" (Cloos, 1983) that encompasses coherent blocks of widely varying sizes (10^{-2} to 10^4 m) of greywacke (lithic-rich sandstone), chert, and minor high-grade metamorphics and ultramafics. At our site (and elsewhere within the Central Belt [Cloos, 1982]) greywacke is the most common block by exposed area (Lovill et al., 2018). The mélange matrix is colloquially called *blue goo*, due its hue in a reduced state and its viscous-like rheology in the near surface. Previous mineralogical studies near the site indicated that the matrix is primarily quartz, albite, chlorite, and phengitic white mica with rare kaolinite, pumpellyite, and lawsonite (Cloos, 1983). Although better known for its high-grade (blueschist) blocks, the
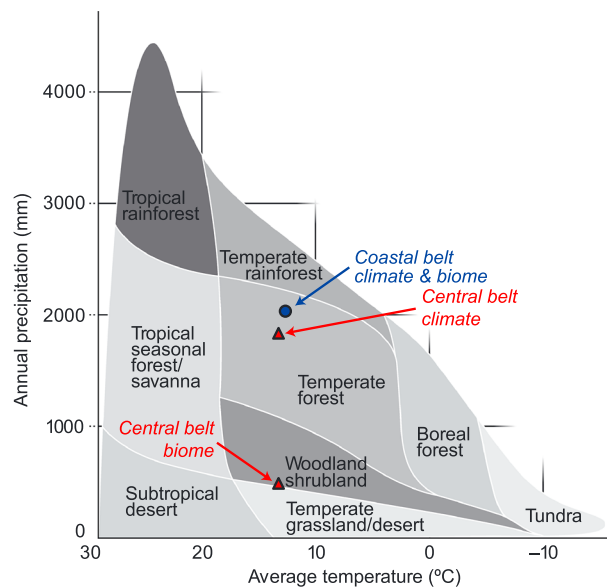
Figure 4. Global delineation of biome type as a function of mean annual precipitation and temperature. The average climate of the Coastal Belt (Angelo; blue circle) and Central Belt (Sagehorn; red triangle) study sites is associated with temperate forests, consistent with the ecosystem inhabiting the Coastal Belt. In contrast, the actual Central Belt biome is woodland/shrubland/grassland, denoted with the lower red triangle. Biome delineations based on Ricklefs (2008) and Whittaker (1975). Greater interception at the Coastal Belt results in nearly identical precipitation at the ground surface, as discussed in text.

pelitic matrix is the primary component of the Central Belt mélange (Cloos, 1983).

2.4. Soils

Soils at the Coastal Belt site are classified as alfisols (Rittiman & Thorson, 2001), consistent with our field observations. At Rivendell, the soil is thin where the slope steepens near the channel and generally thicker (30–50 cm) toward the topographic divide (Oshun et al., 2016). Augering and digging explorations indicate that the surface organic horizon is 5 cm thick. Below lies a massive or poorly sorted, yellow-brown layer rich in centimeter-scale colluvial fragments of argillite and sandstone that lacks clear horizonation. Rock fragments typically have red and brown oxide staining on their exteriors and on internal fracture surfaces. Visible macropores are common, most likely recording root casts and burrows by animals and insects. Despite originating from argillite bedrock, the soil does not experience seasonal deep cracking or other obvious shrink-swell features. The transition between this mobile soil and intact, physically immobile saprolite is typically abrupt and readily identifiable in road cuts or soil pits via poorly sorted colluvium overlying coherent argillite that exhibits throughgoing networks of millimeter- and centimeter-scale fractures and occasional larger-scale bedding planes. Observed processes that collectively mix and transport soil at Rivendell include ground-wasp nesting, animal burrowing, tree throw, rain splash, and during colder winter days the formation of ice pedestals that loft particles downslope.

Soils within the savanna-woodland developed on mélange matrix at the Central Belt site are classified as mollisols (Rittiman & Thorson, 2001), in agreement with observations from ~30 pits and augered boreholes along the topographic divide within the oak-grassland areas. A ~30-cm-thick brown-black organic-rich granular mineral A horizon abruptly overlies a yellow-gray, massive 10- to 20-cm-thick Bt horizon with higher clay content. There is usually an increase in large rock fragments at the Bt—C horizon boundary, and the matrix and rock fragments become less yellow-red and more gray-black-blue in hue. It is not uncommon to find fragments of numerous lithologies (primarily greywacke, chert, and argillite) within a single soil pit at the topographic divide. Here, too, we observe no desiccation cracks on the ground surface in summer. Saturated hydraulic conductivity is high in the near surface (exceeding 10^{-4} cm/s and comparable to maximum hourly rainfall intensities observed since the deployment of a precipitation gauge in 2015) and decreases with depth, reaching lower values (~10^{-5} cm/s) in the upper saprolite (Dralle et al., 2018). Local soil transport occurs via gopher burrowing, wasp nesting, rainsplash, overland flow wash, and (accompanying Euro-American settlement) pig rooting.

2.5. Regional Uplift and Geomorphology

The northward migrating Mendocino Triple Junction was at the latitude of the study area approximately 3 Ma (Atwater & Stock, 1998), and fluvial-marine deposit transitions suggest that the land emerged from sea level at this time (Lock et al., 2006). High regional uplift rates continue to drive rapid river incision in the Northern California Coast Ranges, creating ridge and valley topography. At the study watersheds, prominent local knickpoints (short, steep reaches) are present along the main stem channels (Lovill et al., 2018). Rivendell lies below a major knickpoint on Elder Creek (in the Coastal Belt), which Seidl and Dietrich (1992) proposed originated at the junction with the South Fork Eel and propagated upslope. In contrast, our intensively studied hillslope at Sagehorn in the Central Belt lies above a major apparently stationary knickpoint interpreted to arise from a large resistant block within the mélange encountered by the main stem during incision (as evidenced by a large continuous outcrop on the hillslope adjacent to the knickpoint). This may be one factor contributing to the generally gentler topography within Dry Creek (Central Belt) than in Elder Creek (Coastal belt; Table 1). Within Elder Creek, Holocene fluvial incision rates were ~0.2 mm/year, and during wetter conditions in the Pleistocene, landscape-averaged erosion rates were ~0.4 mm/year (Fuller et al., 2009). Dry Creek's basin-wide cosmogenic nuclide-inferred erosion rate (see

Table 1
Catchment Physiographic and Vegetation Characteristics

	Elder Creek (Angelo; Coastal Belt)	Dry Creek (Sagehorn; Central Belt)
Catchment mouth location	39.7284°, −123.6477°	39.5754°, −123.4642°
Drainage area (km^2)	16.97	3.54
Elevation (max, mean, min; m.a.s.l.)	1,285, 849, 412	905, 733, 593
Geomorphic channel drainage density (km/km^2)[a]	7.9	16.9
Upslope contributing area at channel head (m^2)[a]	6,180	1,085
Canopy cover (mean, median ± 1 s.d. %)[b]	89, 93 ± 12	21, 11 ± 19
Mean hillslope gradient (%)[c]	50.4	27.9
Lithology (see Table 3 for more detail)	Argillite (mudstone), greywacke (sandstone), minor conglomerate	Argillaceous-matrix chaotic mélange containing blocks of sandstone, chert, and various high-grade metamorphics
Erosion rate (mm/year)	0.2 (Holocene)[d] 0.4 (Pleistocene)[d]	0.12 ± 0.01[e] (0.16 ± 0.02 in neighboring Hank Creek)[e]
Vegetation communities	**Mixed broadleaf-needleleaf evergreen forest (north-facing slopes, valleys)[f]:** Douglas fir (*P. menziesii*) Tan oak (*N. densiflorus*) Live Oak (*Q. chrysolepis, spp.*) Madrone (*A. menziesii*) California Bay (*U. californica*) **Understory:** Poison oak (*T. diversilobum*) Oregon grape (*B. nervosa*) Huckleberry (*V. parvifolium*) Ferns (*spp.*) **Riparian:** Alder (*Alnus spp.*) Bigleaf maple (*A. macrophyllum*) **Strath terraces** Oregon white oak (*Q. garryana*) Native perennial and invasive annual grasses **Chaparral (south-facing slopes, higher elevation):** Manzanita (*Arctostaphylos spp.*) Live oak (*Quercus spp.*) Chamise (*A. fasciculatum*) Ceanothus (*Ceanothus spp.*)	**Annual grass deciduous oak savanna-woodland (mélange)[g]:** **Woody plants:** Oregon white oak (*Q. garryana*) Minor California black oak (*Q. kellogii*) and buckeye (*A. californica*) Manzanita (*Arctostaphylos spp.*) **Herbaceous cover:** Slender oat (*A. barbata*) Foxtail barley (*H. murinum*) Filaree (*E. cicutarium*) Medusahead (*T. caput-medusae*) Velvet grass (*H. lanatus*) Italian thistle (*C. pycnocephalus*) **Riparian:** Oregon ash (*F. latifolia*) Bigleaf maple (*A. macrophyllum*) *Large sandstone blocks have similar vegetation community as Elder Creek*

[a]Lovill et al. (2018). [b]Calculated from National Land Cover analytical tree canopy cover data set. [c]Calculated from 1-m-pixel-size NCALM LIDAR data set. [d]Fuller et al. (2009). [e]Determined in this study using cosmogenic ^{26}Al; see section 3. [f]See also Johnson (1979). [g]See also Hahm, Dralle, et al. (2017) and Hahm et al. (2018).

section 3) is 0.12 ± 0.01 mm/year, about half that of Elder Creek, consistent with a decline in modeled regional rock uplift rates at the more southern location of Dry Creek (Lock et al., 2006) combined with lower erosion rates locally, above the prominent knickpoint (Lovill et al., 2018).

The generally weak bedrock of the Franciscan results in numerous earthflows within the Central Belt (Mackey & Roering, 2011; Roering et al., 2009, 2015) and deep-seated landslides and debris flows in the Coastal Belt (Stock et al., 2005). The Dry Creek watershed exhibits widespread earthflow topography (lumpy, "melted ice cream" appearance [Kelsey, 1978]), yet few flows are presently active and the topography may be largely relict, perhaps due to reduced river incision upslope of the knickpoint. This would be consistent with the observations of Bennett et al. (2016), who noted the preponderance of active earthflows below

Table 2
Historical Climate

Site	Mean annual precipitation (mm)	Mean annual temperature (C)	Time range	Reference
Angelo	2,032		1900 to 1963	(Rantz, 1968)
	2,156		1946 to 1976	(Johnson, 1979)
	1,893		1985 to 2007	Peter Steel, pers. comm., 2016
	2,042	12.4	1981 to 2010	PRISM
Sagehorn	1,524–1,778		1900 to 1963	(Rantz, 1968)
	1,790		1961 to 1976	Interpolated COOP stations[a]
	1,811	13.3	1981 to 2010	PRISM

[a]In the 15-year period from 1961 and 1976, two formerly active weather stations in Branscomb and Willits, CA, recorded 2,190 and 1,389 mm of average annual precipitation, respectively (data from NOAA.gov; COOP IDs: 041046 and 049684, elevations: 445 and 412 m, 25 km NW and 20 km SW of the site, respectively).

knickpoints across the mélange and interpreted the relative lack of active earthflows above knickpoints to result in the preservation of relict terrain in headwater catchments of the Eel River watershed.

2.6. Vegetation

The vegetation communities across the two sites are starkly different (see species lists in Table 1, maps and photos in Figures 2 and 3, and early descriptions of the region in Clark, 1937). Angelo (in the Coastal Belt) is characterized by a mixed broadleaf-needleleaf evergreen forest that grades into chaparral at higher elevations and on some south-facing slopes. Douglas fir (*Pseudotsuga menziesii*) is the dominant canopy-emergent species on north-facing slopes and in tributary valleys on south-facing slopes and is typically associated with tan oak (*Notholithocarpus densiflorus*), live oaks (*Quercus chrysolepis* and *Quercus agrifolia*), Pacific madrone (*Arbutus menziesii*), and California bay laurel (*Umbellularia californica*). Coast Redwood (*Sequoia sempervirens*) is not present in the Elder Creek study watershed but is common elsewhere at Angelo and the Coastal Belt in areas more subject to fog. The spatial extent of the Douglas fir may partly be a relic of the practice of Native American burning, which reduced the extent of fir relative to the hardwood forests (Johnson, 1979).

Table 3
Franciscan Geology of the Northern California Coast Ranges

	Coastal Belt	Central Belt
Lithology	Interbedded argillite, greywacke, minor conglomerate ("broken formation")	Argillite-matrix mélange with blocks (primarily greywacke, chert, minor greenstone, blueschist, eclogite, limestone)
Age	Paleocene to Eocene	Jurassic to Paleocene
Interpreted formation	Deformed turbidite sedimentary deposits	Subduction-complex flow mélange
Metamorphic facies	Zeolite	Pumpellyite
Approximate burial *P–T*	1 kbar, <175 °C	3–10 kbar, 100–250 °C
Mineralogy	Argillite: quartz, albite, illite, chlorite, muscovite, microcline, kaolinite, calcite, smectite, anatase, iron oxides, and pyrite. Greywacke: feldspar, quartz, micas, lithics, and some prehnite. Abundant laumontite veins	Mélange matrix: quartz, albite, microcline, muscovite, chlorite, illite, titanite, minor gypsum, pumpellyite and lawsonite, rare kaolinite, and locally aragonite/calcite. Lacks laumontite
Notes	Argillite undergoes disaggregation upon wetting and drying cycles; open fractures above fresh bedrock	Mélange matrix deforms in near surface ("blue goo"); tendency to seal fractures

Note. References: this study; Cloos, 1982; Ernst & McLaughlin, 2012; Gu et al., 2016; Jayko et al., 1989; Kim et al., 2014.

In contrast, Sagehorn, in the Central Belt, is predominantly inhabited by winter deciduous oaks and annual grasses. The water limitation-tolerant Oregon white oak (also known as Garry oak; *Quercus garryana*) is the dominant species (Hahm et al., 2018) and is concentrated with higher density on north-facing slopes, occasionally forming woodlands with contiguous canopy. Dense evergreen forest areas without an herbaceous understory are found on large sandstone blocks, dominated by Pacific madrone and Douglas fir. California black oak (*Quercus kelloggii*) is common along ecotones, which are typically abrupt between grassland and evergreen forest but diffuse between grassland and oak woodland. Rare ultramafic and high-grade metamorphic blocks (order 10 m across) outcrop as barrens devoid of soil and host rare endemic species.

3. Methods

Here we outline the methods employed to track water as it moves through the subsurface to streams, to document its storage within the subsurface in relation to the structure of the critical zone, and then to quantify plant community distribution and water availability.

3.1. Stream Runoff

Stream runoff at the Coastal Belt site is measured by the U.S. Geological Survey (USGS Gauge 11475560, Elder Creek near Branscomb, CA; upstream area 16.8 km^2), ~200 m upstream from the base of the Rivendell study hillslope near the confluence of the creek with the South Fork Eel River. During the study period, streamflow was gauged by the USGS 5–10 times per year, and the USGS estimates 5–10% accuracy for discharge. At the Central Belt mélange site, we measure stage in the channel of Dry Creek near its mouth (~1,400 m downstream from the base of the study hillslope; upstream area 3.46 km^2) and calculate runoff from a rating curve established from >20 measurements spanning discharges of less than 0.001 to greater than 10 m^3/s. Based on the quality of the rating curve and precision of the stage recorder (see below), we estimate 5–10% accuracy for the Dry Creek discharge record.

3.2. Precipitation and Interception

Precipitation is measured with unshielded tipping-bucket rain gauges (Model TB4, Hyquest Solutions). The manufacturer-provided measurement accuracy is better than ±3% given the intensity of rainfall experienced at the site. We perform three adjustment procedures that account for (1) wind-induced undercatch (see supporting information and Allerup & Madsen, 1980; Sevruk, 1982; Yang et al., 1998, for more detail); (2) horizontal variations in rainfall; and (3) data gaps prior to the deployment of gauges. For the Dry Creek catchment (Central Belt), we use one centrally located ridgetop rain gauge (Sagehorn, 715 m a.s.l.), and for the Elder Creek catchment (Coastal Belt), we average precipitation from a gauge located near the mouth ("Angelo Meadow," 405 m a.s.l.) and the headwaters ("Cahto Peak," 1,249 m a.s.l.). The Daymet V3 climate product (https://daymet.ornl.gov/) is used to extend the precipitation time series prior to 2015 at both sites.

We specify a canopy interception storage to account for an initial, event-based "wet-up" period in which rain is captured by the canopy, after which throughfall is equal to the incoming rain intensity (see supporting information and Krygier, 1971; Laio et al., 2001; Miralles et al., 2010; Pypker et al., 2005; Reid & Lewis, 2009, for more detail). The resulting effective precipitation available for storage, evapotranspiration, and runoff, *P*, is used in subsequent analyses.

3.3. Evapotranspiration and Radiation

For each of the two study catchments, we compute potential evapotranspiration (*PET*) with the Hargreaves method (Hargreaves & Samani, 1982, 1985), which requires daily maximum, minimum, and mean temperatures obtained from the weather stations, as well as radiative forcing as a function of latitude and day of year, calculated with scripts from the PyETo Python package. *PET* calculated prior to 2015 relies on Daymet temperature records, which compare well with our local weather stations at both sites during times for which the two data sets overlap. Total solar radiation is measured at Angelo with a Li-Cor LI200X-L Pyranometer. Using historical estimates of actual evapotranspiration (*ET*) from a process-based Moderate Resolution Imaging Spectroradiometer (MODIS)-derived data set described in Ryu et al. (2011) along with Daymet precipitation records, we also plot annual values for each catchment from 2002–2015 in the Budyko space: evaporative fraction (*ET/P*) versus aridity (*PET/P*). *ET* is difficult to quantify over large spatial scales (particularly when *Q* is lacking, as is the case at Dry Creek prior to our installation of a stream gauge

there. The uncertainty of the *ET* data has been evaluated via intercomparison with annual basin water balance and flux tower estimates of *ET* by Ryu et al. (2011), yielding a root-mean-square error of 31% and 26%, respectively (these comparison data sets are also subject to their own inherent uncertainties). For the purposes of this study, we are primarily interested in how differences in subsurface water storage capacity between nearby sites manifest in distinct water balance regimes (and therefore location within the Budyko plot). For this purpose, the Ryu et al. (2011) ET data set, which relies on satellite-based greenness indices, is suitable for intersite comparison even if the absolute location of each catchment within the Budyko space is subject to uncertainty. This is based on the reasonable assumption that greenness scales with ET at each site (i.e., the remotely sensed *ET* signal is correct in relative if not in absolute magnitude). We fit curves to each site in the Budyko space using the analytical formulation of Yang et al. (2008). A single fitting parameter (*n*) is used to describe the shape of the Budyko curve; low values of *n* correspond to catchments with low storage that transform precipitation into runoff efficiently; high values of *n* correspond to catchments with high storage that are able to store precipitation and return it to the atmosphere via evapotranspiration.

3.4. Catchment-Integrated Dynamic Water Storage

Catchment water budgets for the 2017 water year wet season were compared between the two study sites to quantify water storage. The seasonally dynamic water storage is calculated as the change in total catchment storage (ΔS) relative to an October 1 reference state (e.g., Sayama et al., 2011). This date typically coincides with the end of the dry season when annual catchment water storage is at a minimum. Changes in dynamic storage result from gains due to effective precipitation (*P*) and losses to runoff (*Q*) and evapotranspiration, which in the wet season is assumed to be approximately equal to *PET* (we lack daily estimates of actual evapotranspiration for the 2017 water year). Using daily data, we plot cumulative running storage change as $\Delta S = \sum P - \sum Q - \sum PET$. We stop the analysis at the end of May, when the approximation $ET \approx PET$— which assumes high wet season water availability (and an energy-limited state, as is typical in the area [Reid & Lewis, 2009])—becomes increasingly inaccurate. Hence, to the extent that $ET < PET$ in the wet season, the inferred dynamic storage is an underestimate of the actual dynamic storage. Small biased inaccuracies can compound in this running mass balance, requiring high-accuracy input data to produce reasonable dynamic storage estimates. Our analysis benefits from the small areas of the study catchments (which minimize horizontal variation in rainfall and *PET*) and is generally corroborated by hillslope-scale measurements of dynamic storage capacity (discussed below). Dralle et al. (2018) further discuss this method of analysis and its uncertainty.

3.5. Boreholes and Well Casings

Boreholes were drilled during multiple field campaigns at both sites from 2007–2015 to depths typically below the transition from weathered to fresh bedrock (to a maximum of ~30 m; see supporting information for more borehole detail). Recovered material was documented, where feasible, with respect to its color, texture, presence, or absence of minerals indicative of weathering fronts (e.g., pyrite and calcite), fracture density and fill, and water stable isotopic composition (see Hahm, Dietrich, et al., 2017; Oshun et al., 2016; Rempe & Dietrich, 2018). These observations, together with groundwater dynamics and drilling rate-inferred material strength, are used to describe subsurface CZ structure. The depth to fresh bedrock is locally determined by a large increase in material strength, perennial saturation, and lack of mineral weathering. Boreholes were used to monitor groundwater and vadose zone moisture dynamics (see sections below)

3.6. SEM Microstructure Analysis, Mineralogy, and Bulk Geochemistry

To study microstructures that control the porosity and permeability of the fresh mélange matrix of the Central Belt, we collected core on 25 September 2015 and analyzed a sample recovered from 15.3 m below the ground surface in borehole 501 (supporting information Figure S2) at the Indiana University Shale Research Lab (see Schieber, 2010, for more detail). The sample was prepared for scanning electron microscope (SEM) analysis via argon ion milling and scanned at 15.0 kV and 70 Pa.

The mineralogy of both fresh and weathered material obtained from drilling at both sites was measured using X-ray powder diffraction at Indiana University, with quantitative phase determinations via the Rietveld method (see, e.g., Bish & Howard, 1988), normalized to 100%. The relative abundances of illite and smectite were separately estimated via fits to diffraction intensity and are expressed as point-bounded

horizontal bars defining conservative concentration estimates; these phases are not included in the normalization.

To compare parent material bulk composition, we measured the geochemistry of fresh, unweathered bedrock at both sites after pulverization to 200 mesh and analysis via lithium-borate fusion inductively coupled plasma emission spectroscopy at the Bureau Veritas Mineral Laboratories (Vancouver, BC).

3.7. Erosion Rates

We collected in-channel stream sediment from near the mouths of two creeks at Sagehorn (Dry and Hank, which bound the study ridge) within the Central Belt mélange to estimate basin-wide cosmogenic-nuclide-inferred erosion rates (e.g., Granger et al., 1996). We separated quartz from each sample following standard procedures and then isolated Al within the quartz. The concentration of cosmogenic ^{26}Al was measured at the PRIME lab at Purdue University. We then used the CosmoCalc program (Vermeesch, 2007) with Stone's (2000) scaling relations to determine erosion rates (see supporting information for more detail; rates reported in Table 1). Analytical uncertainties from the accelerator mass spectrometer measurement were propagated and are reported with the erosion rate estimates.

3.8. Groundwater Dynamics

We deployed pressure transducers in wells to monitor groundwater table dynamics at Sagehorn in the Central Belt in 2015 (Rivendell's 12 wells in the Coastal Belt were already instrumented before the start of this study). Most wells are outfitted with vented transducers that compensate for atmospheric pressure changes (models CS-450 and CS-451, Campbell Scientific); some are outfitted with offline, internal-battery powered pressure transducers (Solinst Levelogger) that are corrected for atmospheric pressure fluctuations with a nearby, similar-elevation barometric pressure sensor. In some boreholes that were not drilled to the fresh bedrock boundary (MN-1, MS-4, 505, and 508 at Sagehorn) the water table drops below the base of the wells during portions of the year. The accuracy of the Campbell and Solinst transducers are 3.5 and 5 mm, respectively.

3.9. Dissolved Oxygen in Groundwater

We measured dissolved oxygen content in groundwater at Sagehorn in the Central Belt with an optical luminescence sensor (YSI ProODO), with descending depth profiles through the entire undisturbed water column. We waited for readings to stabilize at each measurement depth, which typically took between 30 and 180 s. The instrument measures and adjusts dissolved oxygen percentages to temperature in the water and barometric pressure at the surface. We routinely calibrated the dissolved oxygen meter following manufacturer guidelines with two end-members: water-saturated air, achieved by equilibrating the sensor in a 100% relative humidity sleeve, and 0% dissolved oxygen solution, achieved by dissolving 8–10 g of sodium sulfite in 500 ml of water. The manufacturer provided accuracy when correctly calibrated is ±1%.

3.10. Tree Water Potential

Predawn shoot water potentials were measured near topographic divides at the end of the summer dry season at both sites with a Scholander-type pressure-chamber apparatus (Boyer, 1995; Scholander et al., 1965) following the methods outlined in Hahm et al. (2018); the instrument precision in field conditions is ±0.1 MPa. These measurements are used to compare relative water stress between sites. At the Central Belt site, we measured *Q. garryana* and at the Coastal Belt site we measured three genera of hardwoods (*Q. chrysolepis*, *N. densiflorus*, and *A. menziesii*) as well as the conifer *P. menziesii*. Samples were collected from mature individuals (breast-height diameters typically >25 cm) within 2.5 m of the ground surface at the Central Belt. At the Coastal Belt site, approximately half of the trees sampled had canopies that were inaccessible from the ground, and climbing ropes were used to obtain shoots. These samples' predawn potentials were corrected for the gravitational component of water potential based on their collection height above the ground surface.

3.11. Remotely Sensed Vegetation Analyses
3.11.1. Tree Canopy Cover and Primary Productivity

To explore differences in the forest density between sites, we use the Landsat-derived 2011 analytical Tree Canopy Cover data set (0 to 100% tree canopy cover) provided by the National Land Cover Database (Homer et al., 2015). We also accessed and aggregated the Landsat-derived Net Primary Production

CONUS data set (Robinson et al., 2018) in the Google Earth Engine platform (30-m pixel size) to determine watershed average productivity across the two rock types.

3.11.2. MODIS EVI

We analyzed time series of the MODIS enhanced vegetation index (EVI) MOD13Q1 product (Huete et al., 2002) to assess the impact of CZ water storage dynamics on plant community function and leaf phenology (250-m pixel size). We accessed and aggregated the data using the Google Earth Engine platform and extracted the median EVI pixel value within our study watersheds for the duration of the MODIS program, resulting in 16 complete water years of data. This effectively captured the leaf dynamics of the mixed broadleaf-needleleaf evergreen forest of the Coastal Belt and the herbaceous ground cover (with minor deciduous oak contribution) of the Central Belt (see, e.g., Huete et al., 2006). To explore the seasonal dynamics of ecosystem function, we plot composite annual time series by averaging the median watershed EVI at the same date across all years.

3.11.3. Time Series Landsat and Historical Air Photos

We created a cloud-free mosaicked video of the wider field area (Mendocino County, California) with all available Landsat natural color imagery in the Google Earth Engine platform (supporting information Movie S1) to visualize boundaries between vegetation types through time. We also analyzed historical air photos of the Central Belt site (provided by the UC Santa Barbara Maps and Imagery library) and more recent orthoimagery from the National Agriculture Imagery Program.

4. Results

Results are organized around a description of subsurface critical zone structure, runoff pathways, and water storage at each site, followed by a comparison of plant community distribution, function, and water status. Some of the descriptions of subsurface structure and the hydrologic cycle, particularly for the Coastal Belt, synthesize many previously published works from the Eel River Critical Zone Observatory not previously collectively summarized. These descriptions (with appropriate citations) are combined together with new results here in order to provide a complete, stand-alone portrait of the site. They are then followed by a parallel description of the Central Belt. The common descriptions of both sites lay the foundation for the synthesis of subsurface weathering zone patterns, water storage, and surface ecosystems.

4.1. Coastal Belt (Rivendell Unit Hillslope and Elder Creek)

4.1.1. Subsurface Critical Zone Structure

The Coastal Belt is pervasively fractured and consists of turbidites—packages of interbedded mudstones, sandstones, and conglomerate—which are typically decimeters to meters thick. Extensive drilling shows that the weathering profile structure varies systematically across the landscape (Rempe & Dietrich, 2014, 2018; Salve et al., 2012). Unweathered bedrock is exposed at the ground surface in Elder Creek and the South Fork Eel River. The depth to fresh bedrock increases from about 4 m just above the channel to ~30 m at the hillslope divide (Figure 5; Rempe & Dietrich, 2018). Just below the soil, weathering has generated about 1 to 2 m of saprolite (a material with soil-like properties that retains relict-rock structure). A highly fractured and oxidized weathered bedrock zone lies between the saprolite and unweathered bedrock. Roots were observed to 16-m depth during drilling.

4.1.2. Runoff Pathways and Water Storage

At the start of the wet season, precipitation transits through the mixed broadleaf-needleleaf evergreen forest and then flows vertically as unsaturated flow through the highly conductive soil, saprolite, and weathered and fractured bedrock. A seasonal wetting front advances through the soil, saprolite, and weathered rock and replenishes a vadose zone storage deficit caused primarily by evapotranspiration in the preceding dry season (Rempe & Dietrich, 2018; Salve et al., 2012). Across Rivendell, up to 60 ± 17 mm (avg. $\pm$ 1 s.d.) of water is seasonally stored within the soil, and 280 ± 140 mm is stored as rock moisture—exchangeable water stored in the unsaturated zone in weathered bedrock (which includes saprolite; Rempe & Dietrich, 2018).

At individual wells the annual maximum rock moisture content was the same in successive years, despite a wide range in precipitation (Rempe & Dietrich, 2018). Total rock moisture content increases upslope, consistent with increasing weathered bedrock thickness upslope (Figure 5). Once the maximum storage capacity is reached, further rainwater inputs induce water transport deeper along fractures, recharging the underlying groundwater (Rempe & Dietrich, 2018). Minor early wet season groundwater response occurs in some
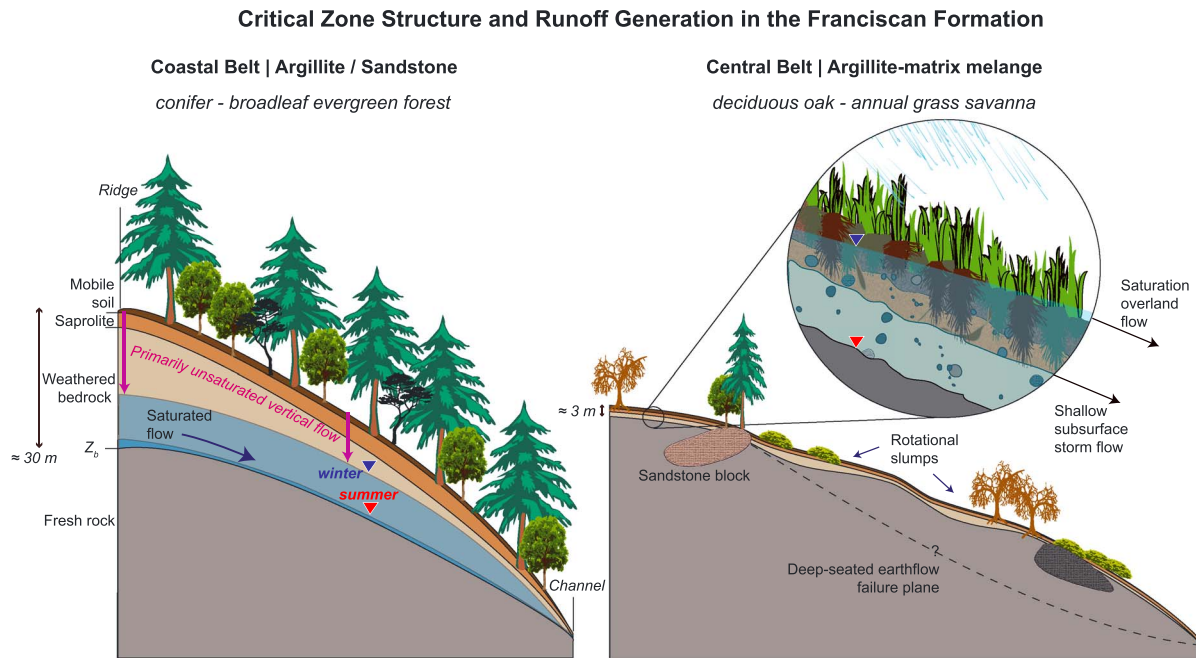
Critical Zone Structure and Runoff Generation in the Franciscan Formation

Figure 5. Schematic cross sections of hillslopes in the Coastal Belt (left) and Central Belt (right) of the Franciscan Complex, highlighting contrasting critical zone structure, runoff pathways, vegetation distribution, and topography. End of winter and end of summer water table positions shown with inverted blue and red triangles, respectively. Runoff in Coastal Belt is generated from saturated flow through fractures in the deep, weathered rock zone that thickens toward the topographic divide. In the Central Belt, the CZ is approximately tenfold thinner at the topographic divide. Many winter storms completely saturate the subsurface, resulting in quick shallow subsurface storm flow through macropores and widespread saturation overland flow. Figure not to scale.

wells and has been interpreted to record local fracture flow that bypassed the rock moisture reservoir (Salve et al., 2012).

Low conductivity, perennially saturated fresh bedrock at the base of the weathering profile causes winter recharge to develop as a seasonal groundwater within the weathered bedrock (Salve et al., 2012). As Figure 5 illustrates, the top surface of low-permeability fresh bedrock, defined as Z_b (sensu Rempe & Dietrich, 2014), slopes toward the adjacent channel, and groundwater flows laterally above it through a dense fracture network. Upslope, depending on the particular location and storm magnitude frequency, it takes between ~200 and 700 mm of cumulative water year rain for infiltrating water to elevate the rock moisture and then pass water to the water table, causing a switch from its slow dry season decline to a more rapid wet season response (Rempe & Dietrich, 2018; supporting information Figure S3).

At the end of the wet season, groundwater recedes, exhibiting a slow decline through the dry summer (Figure 6). Drainage of groundwater from the weathered, fractured bedrock zone sustains perennial flow in Elder Creek (Lovill et al., 2018): Runoff is low but persistent in the summer dry season (on average ~5 to 10 mm/month from June to September).

4.1.3. Catchment-Wide Seasonal Dynamic Water Storage

Figure 7 plots the 2017 water year catchment-integrated dynamic water storage as a residual of the balance between cumulative precipitation, runoff, and potential evaporation. The first major storms of the 2017 water year delivered ~250 mm of precipitation in early October to mid-October and produced minor stream runoff. *PET* at this time of year is minor and caused little moisture storage change before the arrival of subsequent storms. Subsequent precipitation continued to increase storage in the subsurface throughout the Elder Creek catchment, and the runoff response remained relatively muted until large storms in mid-December (recording the progressive increase in rock moisture storage). By January, increases in cumulative runoff closely tracked increases in the cumulative precipitation curve, and the cumulative storage curve leveled off between ~500 and 700 mm, with transient gains and losses in response to storms. Recession analysis indicates that the dynamic water storage at Elder consists primarily of "indirect" storage, which does not drive streamflow and is mainly held as water below a "field capacity"-like state in soils, saprolite, and
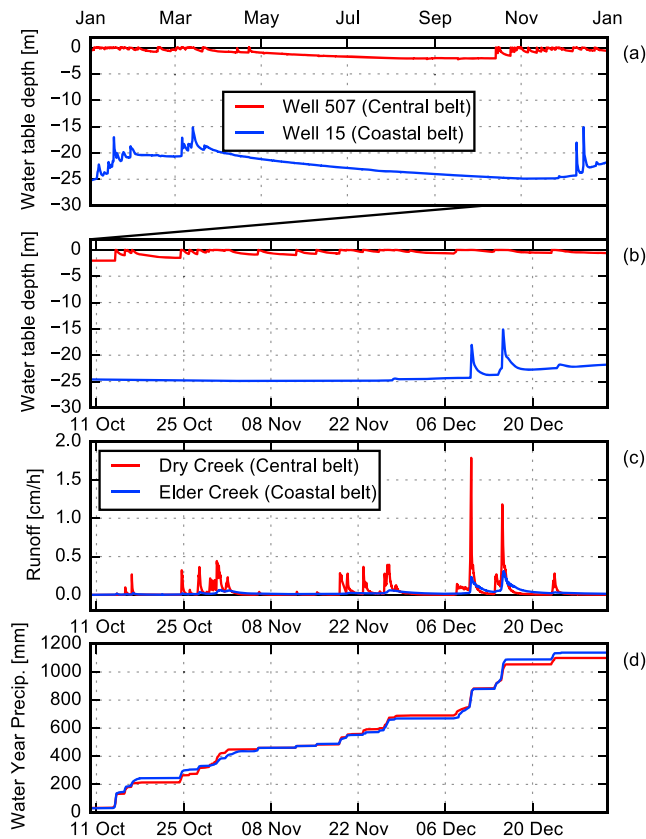
Figure 6. Contrasting groundwater (a, b) and stream (c) responses across sites with different depths to fresh bedrock, Z_b (blue = Coastal Belt; red = Central Belt) to similar precipitation input (d) in 2016. (a) Long dry season recession of groundwater at ridge after last winter rains to contrasting depths. (b) Expanded time series from (a) shows response of groundwater to first rains of wet season. Groundwater in Coastal Belt does not respond until ~700 mm of cumulative precipitation, whereas groundwater in Well 507 rises rapidly to ground surface in first major winter storm, indicating complete saturation of CZ in Central Belt, driving flashy runoff in Dry Creek (c). Variable maximum runoff in Dry Creek with saturated CZ indicates importance of saturation overland flow. Elder Creek response is muted in comparison, with longer recession.

weathered rock and is returned to the atmosphere via transpiration (Dralle et al., 2018; Rempe & Dietrich, 2018).

4.2. Central Belt (Sagehorn Unit Hillslope and Dry Creek)
4.2.1. General Subsurface Critical Zone Structure
At Sagehorn in the Central Belt, fresh mélange matrix is often exposed in channels and drilling observations reveal that it is only 2 to 4 m below the surface at ridgetops. Hence, the subsurface CZ in the mélange is roughly 10 times thinner than in the Coastal Belt (Figure 5). Below the soil lies a ~50-cm-thick, yellow-gray saprolite zone with soil-like texture that grades into a 1- to 2-m-thick, gray-black weathered rock zone. Observed rooting and hyphae depths are confined to the upper few meters. Recovered drill-core and observations of fresh bedrock in stream channels indicate that unweathered mélange matrix has a characteristic blue-black unoxidized hue. Figure 8 reports mineral phases in depth profiles for a borehole at Sagehorn (Central Belt) and Rivendell (Coastal Belt). The uppermost two samples at Sagehorn (from 0.15 and 0.45 m below the surface) and the uppermost sample at Rivendell (from 0.6 m below the surface) were taken from within the mobile regolith (soil). At Sagehorn, the relatively unstable phase gypsum is gone from the soil but present above the fresh bedrock boundary, whereas calcite remains present in the near surface within the soil. There also appears to be a significant enrichment of quartz and depletion of muscovite and chlorite in the uppermost soil relative to the fresh underlying bedrock. Below the depth of the transition to fresh bedrock at Sagehorn (in the Central Belt), there is a higher concentration of chlorite and illite and lower concentration of kaolinite, relative to the mineralogy at Rivendell (in the Coastal Belt). Two samples from Sagehorn (at 1.8-2.1 and 4.0-4.3 m in W506) also exhibited X-ray diffraction patterns consistent with the presence of regularly interstratified (R1) chlorite/smectite, which was not identified in the Rivendell samples. Determining the exact concentration of interstratified chlorite/smectite at Sagehorn is difficult and is not shown in Figure 8; however, it may be between 10% and 20%. Smectite is present throughout the Rivendell profile (in the Coastal Belt) but only appears in the soil at Sagehorn (in the Central Belt).

4.2.2. Subsurface Structure, Runoff Pathways, and Water Storage
Most rain falls directly on low (<20 cm tall) herbaceous ground cover. The soil has a wide distribution of macropores from roots, insects, and burrowing mammals that promote near-surface infiltration and (upon saturation) exfiltration. At the end of the dry season, the seasonally dynamic groundwater is absent: Only residual and essentially stagnant groundwater in the underlying fresh mélange remains at depths greater than 2 to 4 m below the surface (Figure 5). The first major winter storm increases the soil and rock moisture. Further rain leads to groundwater developing in the weathered bedrock zone above the fresh, perennially saturated mélange. Groundwater tables in mélange-dominated wells respond after as little as 50 mm of cumulative precipitation and rise to within 20 cm of the ground surface after only ~100 to 200 mm, effectively saturating the CZ due to the presence of a capillary fringe, implying a dynamic porosity of only ~5% to 10% in the subsurface critical zone.

In contrast to the Coastal Belt, where groundwater remains >10 m below the ground surface at the topographic divide throughout the winter, in the Central Belt the groundwater table frequently reaches the surface during rainfall events (see Figure 6, for detailed dynamics of Well 507 and supporting information Figure S3 for time series of all wells at the site). Stream runoff is generated by subsurface storm flow and saturation overland flow, which quickly deliver water to channels from adjacent hillslopes (Figures 3c and 5). Field observations indicate that during times of sustained mean rainfall intensity exceeding
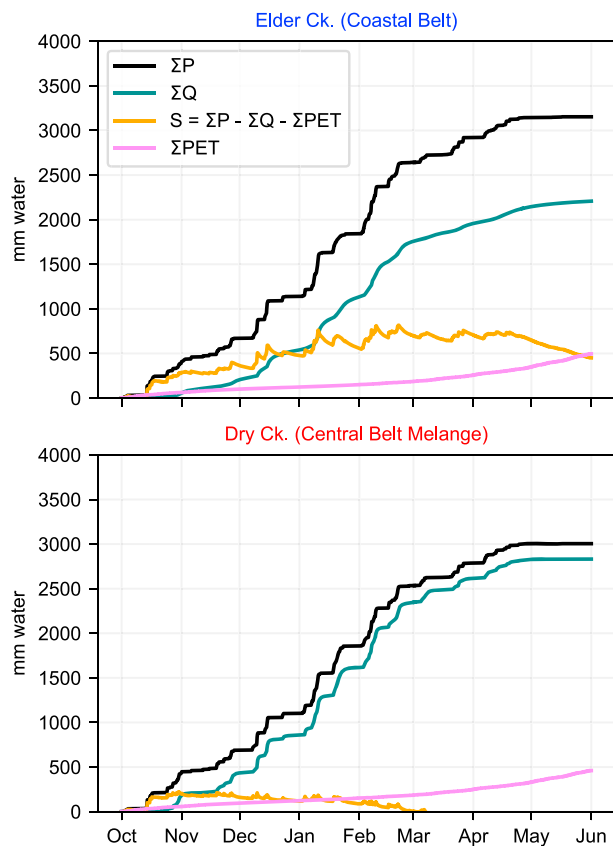
Figure 7. Cumulative precipitation (*P*), runoff (*Q*), potential evapotranspiration (*PET*), and inferred catchment-wide dynamic storage (*S*) in the 2017 water year. The Dry Creek watershed has a factor of approximately four lower catchment-wide dynamic storage than the Elder Creek watershed and reaches a maximum storage sooner into the wet season, resulting in a much higher runoff ratio.

~1 cm/hr, which occurs in many winter storms, saturation overland flow extends to ridgetops across the landscape (see photo in Figure 3d).

In the spring, the seasonally dynamic groundwater levels rapidly decline (supporting information Figure S3). Rapid exhaustion of this shallow storage leads to a lack of baseflow in adjacent streams and a dry channel network in the appropriately named Dry Creek watershed. By 1 August, the water table in the ridgetop Well 507 in the Central Belt mélange has lowered to the fresh bedrock boundary, Z_b, and remains essentially static for the rest of the dry season (Figure 6a), indicative of very low saturated conductivity. The underlying saturated fresh bedrock does not drain significantly on a seasonal timescale and thus does not contribute measureable flow to channels. The dissolved oxygen content was indistinguishable from 0% throughout the groundwater column in Well 507 (except for near the water table surface, which exhibited higher oxygen concentrations) for measurement dates in the 2017 water year (supporting information Figure S4).

SEM imagery of a fresh, deep sample obtained via drilling reveals a heterogeneous fabric of sand-size metamorphic rock fragments, set in a finer-grained matrix composed of <60-μm fine particles that are angular and very poorly sorted (Figure 9). These fine particles are themselves situated within a matrix-supported felted mass of phyllosilicates (likely chlorite) and lack obvious cleavage and foliation at this scale. Interparticle pores (i.e., framework pores) range in size from 10–20 nm, and larger particles may show intraparticle pores in the 10- to 100-nm size range. Due to its low intrinsic porosity, the low-viscosity epoxy resin that was used to stabilize the sample did not penetrate into the sample. Collectively, these observations and the reduced color (blue/gray) reveal the fresh mélange matrix to have very little porosity, likely extremely low saturated conductivity, and minimal groundwater flux—consistent with persistent saturation and low runoff, despite a relatively large hydraulic gradient (20% slope) from ridgetop to channel.

Subsurface heterogeneity results in contrasting hydrologic dynamics over relatively short spatial scales. For example, in the group of three deep wells near the weather station (500, 501, and 502; supporting information Figure S2), which are each ~2 m horizontally from each other and at similar ground surface elevations, a more-than-7-m vertical water table difference is maintained throughout the dry season (supporting information Figure S3) in these adjacent wells. The depth to the perennially saturated zone is 2 to 3 m below the ground surface in wells drilled to 6- to 8-m depth, and 9 to 10 m (Well 501) below the ground surface in a well drilled to 15-m depth. During drilling, we encountered repeated contrasts between soft mélange matrix and hard blocks in this area, suggesting a chaotic subsurface block-in-matrix fabric with extremely low hydraulic conductivity (likely on the order of 10^{-10} cm/s, based on the lack of drainage between wells over the summer). In a sandstone block on the same ridgeline (Well 503; supporting information Figure S2), groundwater behaves in a manner more similar to the Coastal Belt, staying >5 m below the ground surface throughout the wet season and slowly receding throughout the summer (supporting information Figure S3).

4.2.3. Subsurface Structure and Catchment-Wide Seasonal Dynamic Water Storage

Similar to storage in the Elder Creek watershed, Dry Creek storage responds to early rainfall events and exhibits rapid dynamic storage increases as the first rains of the wet season infiltrate into the subsurface (Figure 7). However, after 250 mm of rain, storage (*S*) continues to increase at Elder Creek, whereas subsequent rain at Dry Creek produces only minor, transient increases in storage. Rain inputs rapidly trigger runoff in Dry Creek. As a result, the precipitation ($\sum P$) and runoff ($\sum Q$) curves are coupled (i.e., parallel). The total magnitude of maximum dynamic water storage at Dry Creek is approximately four times lower than Elder Creek, consistent with the differences inferred from the hillslope-scale groundwater and rock moisture storage dynamics. At its peak, the dynamic water storage at Dry Creek primarily occurs as groundwater (the
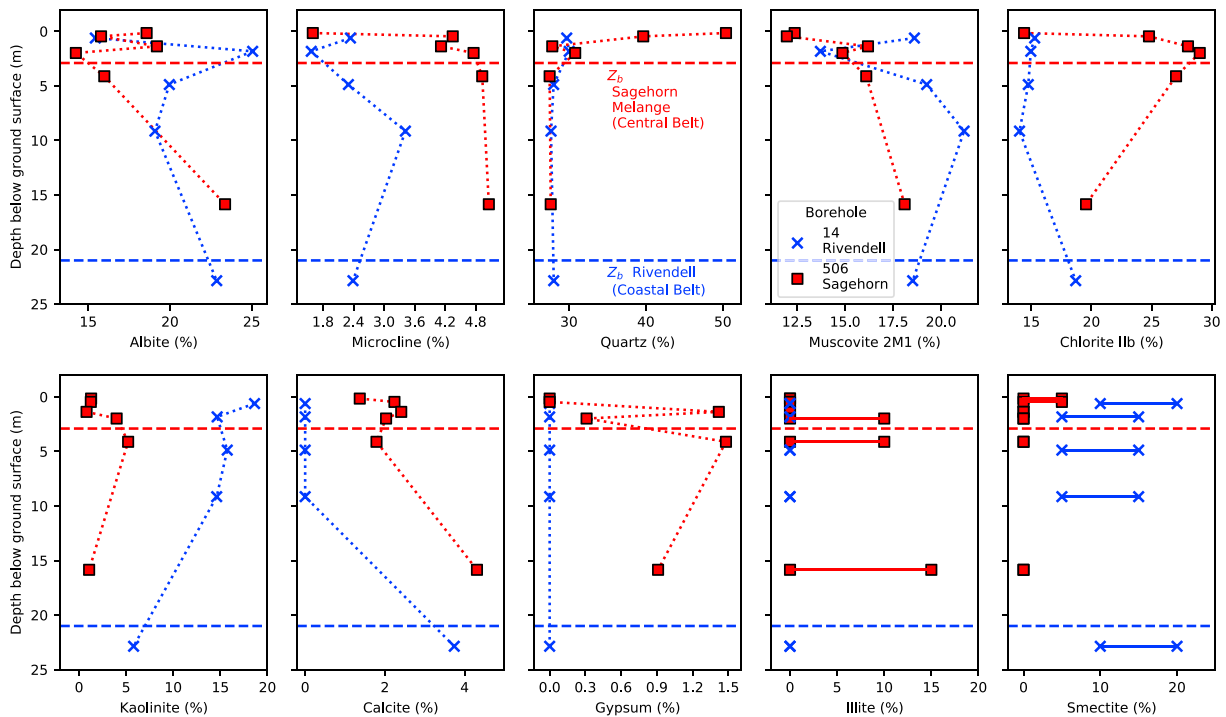
AGU
100
ADVANCING EARTH
AND SPACE SCIENCE

Water Resources Research

10.1029/2018WR023760

Figure 8. Depth profiles of XRD-determined mineral phases. Horizontal dashed lines indicate drilling-inferred transition to fresh bedrock (Z_b) at each borehole (14, blue, Coastal Belt; 506, red, Central Belt). Illite and smectite were separately estimated and not included in the normalization, resulting in some sums exceeding 100% (see section 3). Their concentrations are presented as likely ranges, as denoted by the horizontal lines.

entire subsurface is saturated). The seasonally dynamic storage becomes negative at Dry Creek in March, which is due to $\sum PET$ overestimating actual evapotranspiration as the site becomes water limited.

4.3. Cross-Site Comparison of Forest Density and Productivity

The >200-km-long ecotone that separates mixed broadleaf-needleleaf evergreen forests (in the west) from oak savanna-woodland (in the east) in the Northern California Coast Ranges (Figure 1) generally coincides with the mapped geologic contact separating the Coastal (in the west) and Central (in the east) Belts of the Franciscan (geologic mapping by Jayko et al., 1989; Figure 2). This is consistent with our geologic surveys of the area, independent airborne magnetic surveys (Langenheim et al., 2013), and topography, which indicates a change from the steep-sloped Coastal Belt to gently sloped Central Belt. Across the Elder Creek watershed in the Coastal Belt, the tree canopy cover is 89, 93 ± 12% (mean, median ± 1 s.d.), compared to 21, 11 ± 19% in the Dry Creek watershed in the Central Belt. The larger variance in the Central Belt is attributable to the mosaic of pure grassland and oak woodland, as well as distinct "islands" of mixed broadleaf-needleleaf evergreen forest that abruptly rise from "seas" of grassland and oak savanna. Our local reconnaissance geologic mapping has revealed that these evergreen forest communities occupy large (up to kilometers) blocks of sandstone within the Central Belt. Figure 10 shows one such island plant community assemblage near the mouth of Dry Creek, which has developed on a monolithologic block of lithic-rich sandstone (greywacke), a block type that is common throughout the Central Belt, according to Ernst and McLaughlin (2012), and also a significant constituent of the Coastal Belt. The average remotely sensed and modeled annual net primary productivity between 1986 and 2017 is about twice as high in the Coastal belt forests in the Elder Creek watershed (1.2 ± 0.064 kg C/m^2; mean ± 1 s.d.) than in the Central Belt mélange savanna-woodland in the Dry Creek watershed (0.6 ± 0.037 kg C/m^2).

4.4. Alternative Possible Drivers of Vegetation Patterns

Disturbance, in the form of anthropogenic landscape modification and fire, does not appear to control the distribution of the plant communities. Long-standing fence lines do not coincide with ecotones at our Central Belt site, indicating that preferential grazing does not give rise to the forest and grassland
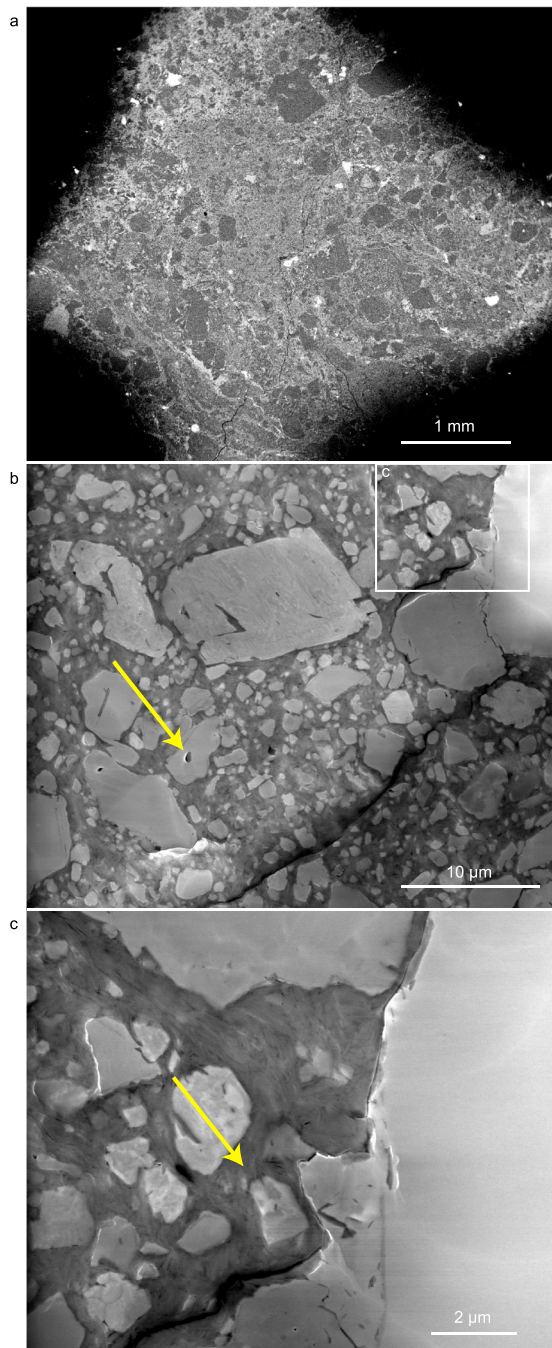
Figure 9. Scanning electron microscope images taken at increasing levels of magnification of fresh mélange matrix. The uppermost image (a, low magnification), shows scattered larger (sand size) particles (mineral and rock fragments) that are suspended in a fine-grained matrix. At intermediate magnification (b), we see larger silt-size particles (also mineral and rock fragments) in a finer matrix. The larger particles may show intra particle pores (yellow arrow). At highest magnification (c), the intraparticle matrix resolves as a felted mass of phyllosilicates (likely chlorite). This phyllosilicate matrix has some intrinsic porosity (interparticle framework pores, yellow arrow), but pores are small (~10–20 nm) and not abundant, and thus permeability is low. Larger open spaces between phyllosilicate matrix and mineral grains are not pores but rather artifacts of sample preparation (beam heating causes shrinkage of phyllosilicate matrix).

transitions. Native Americans practiced a fire management regime that included high-frequency, low-intensity burning to enhance acorn production, improve hunting grounds, and promote desired cultivars for millennia in the area (Johnson, 1979; Lightfoot & Parrish, 2009; Mensing, 2006). However, the response of vegetation on each side of the geologic contact to disturbances like logging and fire indicates that the distribution of plants does not primarily reflect successional stages. Landsat surveillance shows repeated and widespread clearcutting across Mendocino County, CA, within the Coastal Belt forests around the Angelo Coast Range Reserve over the past three decades. Supporting information Movie S1 shows that after a parcel is cut, forest canopy begins to return within years and does not revert to grassland. The 12,536-acre 2014 Lodge Lightning Complex fire that burned just north of Elder Creek (Coastal Belt) is also visible in the last frame of the Landsat video, and our on-the-ground post-fire recovery observations do not indicate a transition from forest to grassland. The extent of the herbaceous ground cover of the Central Belt has remained essentially static throughout the duration of the Landsat program, and historical air imagery dating from 1941 (supporting information Figure S5) also shows that ecosystem boundaries have remained largely unchanged, in spite of selective logging and a large fire that occurred at Sagehorn (in the Central Belt) in 1950 (the aftermath of which can be seen in the 1952 air photo in supporting information Figure S5b). The air imagery indicates that although forest abundance was higher across the Central Belt site prior to logging and fire, the spatial arrangement of forests do not appear to have shifted (cf. supporting information Figures S5a and S5c).

The bulk elemental chemistry of fresh rock samples from the two sites is broadly similar and consistent with typical compositions of fine-grained siliciclastic rock (supporting information Table S1). The Central Belt mélange tends to have higher Mg compared to the Coastal Belt, in agreement with the difference between the average compositions of shale and metamorphosed shale (Gromet et al., 1984; supporting information Table S1). Neither site has exceedingly high concentrations of elements associated with ultramafic toxicity (Kruckeberg, 2004), although the mélange does have higher Ni concentrations (~200 ppm) than the Coastal Belt (~60 ppm). Both sites have relatively abundant concentrations of the plant-limiting rock-derived nutrient phosphorus (>0.2 weight % P_2O_5; compare with concentrations of <0.05 weight % inferred to be limiting in Hahm et al., 2014). We therefore rule out the possibility that the sharp ecotones arise from historical land use, fire disturbance, or parent material geochemical composition.

After lithology, the second strongest apparent control on plant community distribution is hillslope aspect. At both sites, tree canopy cover is denser on north-facing (poleward) slopes. Within the Dry Creek watershed in the Central Belt, north-facing (315° to 45° azimuth) tree canopy cover is 25.9 ± 20.5% (mean ± 1 s.d.) and south facing (135° to 225°) is 12.6 ± 13.0%. Within the Elder Creek watershed in the Coastal Belt north-facing canopy cover is 92.9 ± 5.9% and south-facing canopy cover is 81.3 ± 19.4%. Poleward facing slopes are typically associated with lower solar radiation and evaporative demand, which lead to higher water availability. This could suggest that the higher tree canopy cover on north-facing slopes at both sites indicates that vegetation is more water limited than energy limited. However, fires were common at both sites (Hahm

Figure 10. Perspective view near the mouth of Dry Creek at the Central Belt site. Red line denotes contact between sandstone block (covered with mixed broadleaf-needleleaf evergreen forest) and mélange matrix (with primarily annual herbaceous ground cover) from reconnaissance geologic mapping. Scale varies in this west-looking view; sandstone block is ~750 m across in W-E direction. Google Earth imagery date 30 May 2014, eye-altitude 1.5 km, 1.5× vertical exaggeration.

et al., 2018; Johnson, 1979), and drier vegetation on south-facing slopes may have burned more readily, also potentially explaining the aspect-related canopy cover differences.

4.4.1. Plant Ecosystem Function in Relation to Energy and Water Availability

Composite annual time series of the EVI highlight contrasting phenological patterns in the Central and Coastal Belts in response to similar climatic forcing (Figure 11). Radiation is approximately 5 times higher in the summer than the winter, due to the effects of longer days, higher solar angle of incidence, and lower cloud cover. In the Central Belt mélange, peak EVI occurs in early May, approximately 45 days before the summer solstice and peak incoming solar radiation. This typically coincides with the last significant wet season precipitation event. The subsequent summer decline in EVI is consistent with senescence of annual grasses and dormancy in perennial grasses, both of which also respond rapidly to the first winter rains in early October. The interannual variation in EVI (1 s.d. vertical bars in Figure 11) in the Central Belt is highest in the spring and fall, indicating sensitivity to high interannual variation in late and early wet season precipitation (Figure 11a). In contrast, at the Coastal Belt site, EVI peaks with the summer solstice and closely tracks incoming solar radiation throughout the year, reaching a minimum during the winter solstice (Figure 11). Unlike the Central Belt, the interannual variation is relatively constant throughout the year in the Coastal Belt.

The sustained evergreen transpiration within the Elder Creek watershed (Coastal Belt) results in an evaporative fraction (ET/P) that is consistently larger than the Dry Creek watershed (Central Belt) for similar values of aridity (PET/P; Figure 12a). The corresponding distributions of water year total P, ET, and PET (Figure 12b) across multiple years (2002–2015) reveal that despite high annual variations in P, ET is relatively constant from year to year at both sites, in general agreement with the similar annual phenological patterns in Figure 11.

4.4.2. End of Summer Subsurface Water Availability

Predawn water potential in Douglas fir, live oak, madrone, and tan oak in upslope positions in the Coastal Belt in mid-September, 2017, was -1.60 ± 0.08 MPa; $n = 22$ (mean $\pm$ s.e.m.; n = number of trees), nearly 1 MPa higher than the Oregon white oak in the Central Belt (-2.46 ± 0.31 MPa; $n = 6$; data for each individual tree are provided in the accompanying data set). This indicates that root zone water availability is much lower in the Central Belt than in the Coastal Belt. Hence, in spite of the much higher canopy density in the Coastal Belt than the Central Belt—and associated high transpiration demand—water potentials are higher in the Coastal Belt than the Central Belt, consistent with a higher amount of subsurface plant available water in the Coastal Belt.

5. Discussion

We found that two compositionally similar lithologies produce radically different subsurface critical zone thickness, water storage capacity, and, consequently, plant-available summer water availability. Here we discuss how these differences control plant assemblages and the partitioning of water between ET and runoff. We also explore possible mechanisms leading to thin versus thick subsurface critical zones in the two rock types.

5.1. Lithologic Controls on Plant Communities: Why a Savanna Occurs Where It Rains Nearly 2 m per Year

Climate monitoring indicates that the two sites receive similar rainfall, yet the Coastal belt supports an evergreen forest that is twice as productive as the annual grassland savanna found in the Central Belt. Climatic conditions are expected to favor temperate forests (Figure 4). Due to the deeper critical zone, hillslopes in the
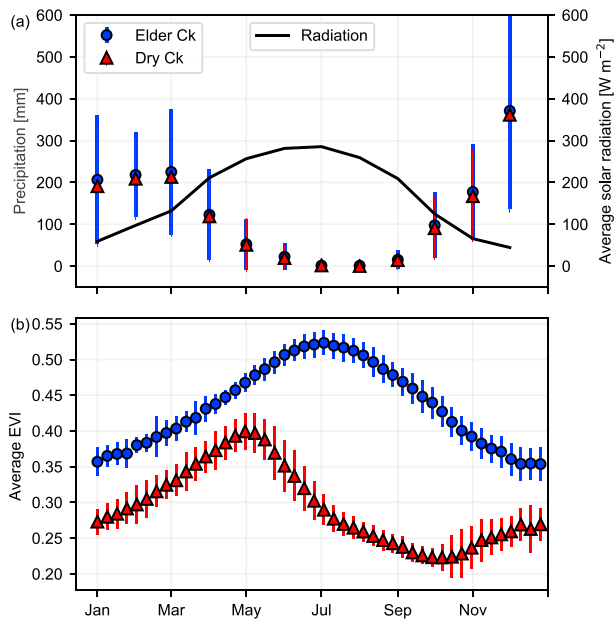
Figure 11. Composite annual time series of (a) energy (radiation measured at Angelo in the Coastal Belt) and water delivery reveal that in spite of similar climate, distinct subsurface CZ water storage capacity, and plant water availability result in distinct annual phenological trends, as shown via the enhanced vegetation index (EVI; b) from MODIS within the Elder Creek (Coastal Belt) and Dry Creek (Central Belt) watersheds. Vertical bars = 1 standard deviation.

Coastal Belt store much more precipitation as plant-available rock moisture than the Central Belt (Figure 7), resulting in greater summer water availability and higher predawn water potential. At both sites, augering and drilling observations of roots, as well as repeat neutron probe measurements (Hahm, Rempe, et al., 2017; Rempe & Dietrich, 2018), indicate that plants use soil and rock moisture. Sap flow rates in Oregon white oak in the Central Belt remain high throughout the summer dry season, declining to only 70–90% of their maximum with shorter day lengths in the autumn (Hahm et al., 2018). In the Coastal Belt, madrone—and to a lesser degree live oak—similarly transpire at high rates in September, whereas Douglas fir exhibits greater decline during the summer (Link et al., 2014). The continued transpiration results in progressive depletion of subsurface moisture storage and associated declines in water potential throughout the summer. The distinct predawn water potentials between the sites presumably reflect differences in both subsurface plant-available water as well as the ability of each plant community to draw down that water: The oaks that inhabit the mélange are able to pull harder, explaining their ability to persist in the water-limited subsurface critical zone of the Central Belt.

The low storage capacity at the Central Belt arises due to the relatively shallow depth of weathering, indicated by perennially saturated, fresh mélange matrix just a few meters from the ground surface. The shallow weathering in the Central Belt mélange results in a critical zone that quickly saturates and sheds most winter rainfall, and then becomes very dry in the summer, supporting only annual grasses that die in shortly after the wet season and scattered oaks that can continue to draw down moisture at extremely low water potentials.

A second factor that likely limits the establishment of forests at Sagehorn is the complete saturation of the Central Belt's thin subsurface CZ with each major winter storm event (Figure 6). This results in an upland landscape that is effectively flooded for almost half of the year (Figure 6). Saturation promotes an anoxic rhizosphere, due to the consumption of oxygen in respiration and the much lower diffusion coefficient of oxygen in liquid water relative to air (Armstrong, 1980), as observed in the winter groundwater of Well 507 at
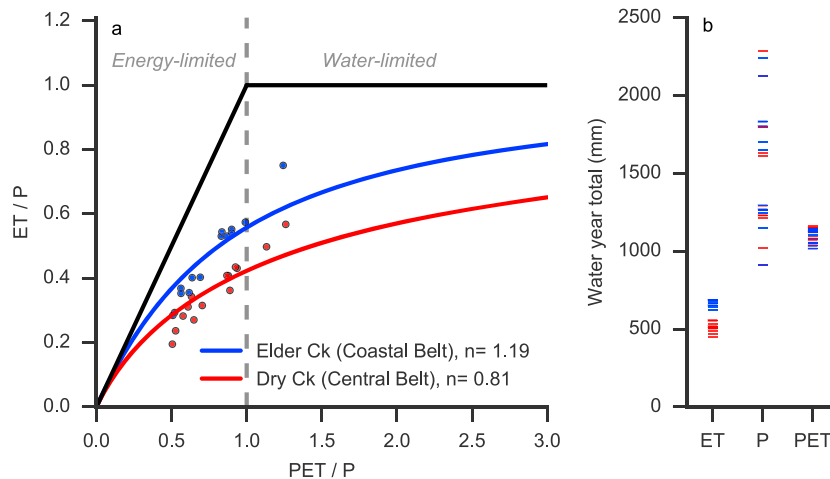

Figure 12. Energy and water balances of each site depicted within the traditional Budyko framework indicate that the Elder Creek catchment partitions more incoming precipitation into evapotranspiration (*ET*; remotely sensed, and including interception losses; see Ryu et al., 2011) than Dry Creek, in spite of similar *P* and potential evapotranspiration (*PET*) between the sites. Each point (a) and horizontal line (b) represent a single water year, from 2002–2015. Lines fit (and reported parameter *n*) according to equation described in Yang et al. (2008).

Sagehorn in the Central Belt (supporting information Figure S4). *P. menziesii* seedlings (the widespread conifer within Elder Creek in the Coastal Belt) respond negatively to even short periods (1 day) of saturation (Minore, 1968; Zaerr, 1983). This indicates that a recruitment bottleneck for *P. menziesii* due to wet season saturation likely exists in the Central Belt mélange in addition to low dry season water availability. The lack of conifers on poorly drained sheared mudstone with clay-rich argillic horizons in the Franciscan Formation was noted by Popenoe et al. (1992), who also suggested that poor drainage would inhibit *P. menziesii* establishment.

Our observations suggest that vegetation inhabiting the Central Belt mélange must overcome the challenge of a CZ that is both very dry (in summer) and very wet (in winter). Species inhabiting this landscape need to be water limitation tolerant and flood tolerant or winter dormant. The annual grass life history strategy is adapted to these conditions; our observations also indicate that remaining native perennial bunchgrasses return year after year in spite of winter water logging (see the extended discussion of the role of annual invasive grasses in the supporting information Text S1, as well as Biswell, 1956; Burcham, 1957; Danielsen & Halvorson, 1991; Davy, 1902; Frenkel, 1977; Gordon et al., 1989; Gordon & Rice, 1993; Hibbs & Yoder, 1993). The dominant tree species inhabiting the mélange matrix, *Q. garryana*, is also well suited to these conditions. It is winter deciduous, with a leaf-off period that closely matches the sustained wet-season subsurface saturation (Hahm et al., 2018) and is known to inhabit riparian areas elsewhere prone to saturation (Stein, 1990). *Q. garryana* is also extremely water limitation tolerant, capable of sustaining high rates of sap flow throughout the summer even as predawn water potentials drop to −3 MPa in some individuals (Hahm et al., 2018). Sap flow is sustained via a low turgor loss point that dynamically adjusts to keep stomata open and investment in an embolism-resistant xylem network (Hahm et al., 2018). These ecophysiological adaptations help to explain the abundance of *Q. garryana* within the mélange.

5.2. An Ecohydrologic Framework for Vegetation Mosaics in Seasonally Dry Environments

The patchy, heterogeneous distribution of ecosystems within areas of similar climate in both seasonally dry California and other Mediterranean climates globally has previously been interpreted to arise due to aspect, nutrient availability (e.g., Hahm et al., 2014), the presence of serpentine (e.g., Kruckeberg, 1985), or pyrodiversity (e.g., Bird et al., 2008; Martin & Sapis, 1991; Trauernicht et al., 2015). Pyrodiversity is defined as "landscape heterogeneity and diverse biota that result from various stages of plant succession as those plants recolonize burned areas" (Lightfoot & Parrish, 2009). Instead of reflecting topographic controls on energy supply, parent material toxins or nutrients, or fire-driven successional stages, we suggest that the diversity in ecosystem function and composition within an area of similar climate can also arise due to CZ-structure-mediated water storage capacity.

In a similar vein to our findings, previous studies have argued that lithologically controlled bedrock permeability can be responsible for differences in seasonal water storage (e.g., Pfister et al., 2017). Ecohydrologic theory also suggests that differences in integrated porosity throughout the subsurface should translate into distinct plant-available water regimes (e.g., Laio et al., 2001; Porporato et al., 2001). In line with this idea, Fellows and Goulden (2016) suggested that low summer plant water use in the high Sierra in glaciated areas may be due to limited subsurface water storage capacity. Studies have also highlighted the importance of soil water storage capacity in affecting water availability and partitioning (e.g., Heilman et al., 2014; Smith et al., 2011), yet there is increasing recognition of the ecohydrological importance and variability of the weathered bedrock below soils: Soils, in contrast to weathered bedrock, vary in thickness over a much smaller range and are commonly thin (<0.5 m) across upland landscapes (Amundson et al., 2015; Schwinning, 2010). The difference in soil thickness—and presumably also the associated soil moisture—between our two sites is minor and not evidently responsible for the large differences in plant water availability. Instead, it is the great difference in the extent and depth of weathering in the underlying bedrock that results in the distinct plant communities.

Quantifying catchment-scale water storage—which we have found useful to scale between the unit hillslope to larger spatial scales—is an active research area in hydrology (McDonnell et al., 2018; McNamara et al., 2011; Tetzlaff et al., 2011). However, we are unaware of studies that have paired these larger-scale catchment storage analyses with detailed subsurface investigation via boreholes to explain plant water availability and distribution. Our study exploits a unit hillslope approach, wherein detailed documentation of critical zone hydrologic functions controlled by the degree and depth of bedrock weathering is used to explain
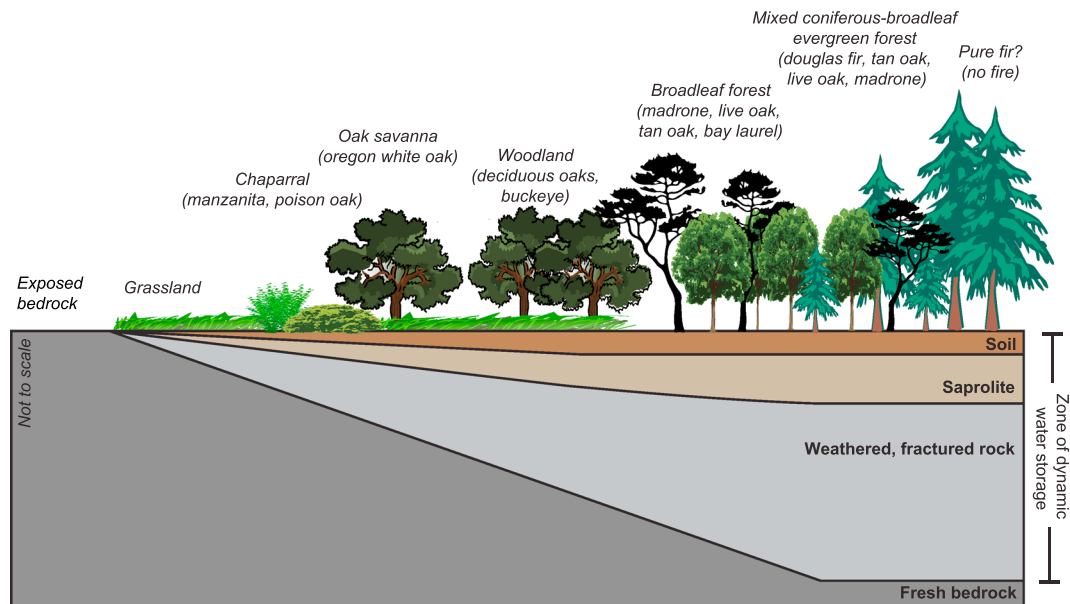
Figure 13. Conceptual cross section illustrating the hypothetical role of critical zone structure in governing water storage and ecosystem composition in the seasonally dry, Northern California Coast Ranges. Topographic position, rainfall, and evaporative demand are assumed constant: only the thickness and corresponding water storage capacity changes from left to right. Although shown as a horizontal surface, this analysis applies to well-drained hillslopes underlain by bedrock, not valley flats where thick colluvium or alluvium may accumulate and seasonal drainage may be poor. Plant variation at far right illustrates possible role of fire exclusion in promoting pure stands of Douglas fir (e.g., Schriver et al., 2018).

regionally extensive (>100 km) contrasts in plant community distributions that covary with lithology. There are limits to the unit hillslope approach, to the extent that the site chosen for intensive study may not be an ideal representation of the larger landscape. However, given the current lack of methodologies to document the extent of the weathered zone and intra-hillslope hydrologic processes at large spatial scales, we suggest that study of a topographically and lithologically representative unit hillslope provides a useful proxy for understanding larger areas.

Figure 13 conceptually summarizes our interpretation that low dynamic water storage capacity arising from thin subsurface critical zones limits the supply of water to plants in the summer dry season. Rainfall is the same across the transect and is sufficient to support the mixed broadleaf-needleleaf evergreen forest found in the Coastal Belt. Where all else is hypothetically equal, a thin CZ with low storage becomes dominated by species that are winter saturation tolerant and more summer water limitation tolerant (at left in Figure 13). This would tend to manifest in lower leaf area, lower summer transpiration, and in general, a lower-productivity plant community. Although our two sites are presented here as general cases of relatively low and high storage capacity—associated with the Central Belt and Coastal Belt, and relatively low and high productivity ecosystems, respectively—the confluence of biota, climate, tectonics, and lithology that influence subsurface CZ structure presumably results in a spectrum of subsurface water storage capacity. Thus, as hypothesized in Figure 13, a subsurface water storage capacity control on ecosystem function may not only be important in creating vegetation mosaics in the Northern California Coast Ranges but in other water-limited seasonally dry environments as well. As the climate warms and habitable plant zones for particular species shift (e.g., Anderson & Ferree, 2010; Kelly & Goulden, 2008), rock type—through its impact on water storage capacity—will likely interact with the effects of climate change in setting future habitat compatibility in these regions.

5.3. Lithologic Controls on the Partitioning Between Evapotranspiration and Runoff

When integrated over an annual cycle, water budgets for most years between 2002 and 2015 plot within the energy-limited side of the Budyko space (Figure 12a). This arises due to the temporal lag between water delivery and water demand in the Mediterranean climate of the study area (e.g., Milly, 1994). This contrasts with the observation that the catchments are more water limited than energy limited in the summer: May–September PET, a metric of atmospheric moisture demand (based on the Hargreaves method) is on average

725 mm at Dry Creek (Central Belt) and 704 mm at Elder Creek (Coastal Belt), exceeding the maximum observed dynamic water storage volumes that could be returned to the atmosphere. This indicates that energy- versus water-limited descriptions for catchments determined from annual water budget analyses may not be useful descriptors of ecosystem water availability at subannual (i.e., seasonal) timescales in strongly seasonal climates, like our Mediterranean study sites.

Variations in the vertical location of the Budyko line—or the amount of water that is returned to the atmosphere for a given dryness index—have been theorized to arise due to differences in subsurface moisture storage (e.g., Milly, 1994; Milly & Dunne, 1994; Porporato et al., 2004; Yang et al., 2008; Rouholahnejad Freund & Kirchner, 2017), but to our knowledge no empirical, comparative study in a seasonally dry climate has probed the entire depth of the critical zone with deep boreholes to show how lithologically controlled differences in bedrock weathering explicitly govern this water partitioning. Our catchment-wide analyses indicate that smaller dynamic storage volumes at Dry Creek (Central Belt) relative to Elder Creek (Coastal Belt) are likely the cause for lower values of ET/P at Dry Creek for the same value of PET/P (Figure 12a). This difference arises due to rock-type governed limitations on CZ water storage capacity.

The idea that subsurface CZ structure can limit dynamic water storage also has implications for the ET response to interannual variations in P. Excess P beyond that required to replenish the dynamic subsurface storage capacity runs off in the winter (as similarly found in and near the Eel River basin by Syvitski & Morehead, 1999, and Sayama et al., 2011, and suggested by Smith et al., 2011, in Idaho [in soils] and Fellows & Goulden, 2016, in the Sierra Nevada). Because it runs off, this excess P does not generate extra plant-available water storage for the following summer. The result is that high year-to-year variations in P at both sites do not result in highly variable ET due to the storage-limited nature of the two study catchments (Figure 12b).

5.4. Development of the Subsurface Critical Zone Structure

Recent theories have identified the importance of tectonics, lithology, and climate in governing the development of the subsurface CZ (Anderson et al., 2013; Lebedeva & Brantley, 2013; Rempe & Dietrich, 2014; Riebe et al., 2017; St. Clair et al., 2015). The thickness of the subsurface CZ is determined by the difference between the ground surface topography and the elevation of the transition from weathered to fresh bedrock. The slope of the fresh bedrock boundary that we observe at our Central Belt mélange site between the ridgetop wells and Dry Creek (supporting information Figure S2) is essentially the same as the slope of the topographic surface, and fresh bedrock outcrops in the channel (i.e., the subsurface CZ is thin), whereas in the Coastal Belt, fresh bedrock also outcrops in the channel, but the fresh bedrock surface slope is considerably less than the average topographic slope, resulting in a thick CZ at the topographic divide. Motivated in part by observations in the Coastal Belt, Rempe and Dietrich (2014) propose that the slope of the fresh bedrock surface may represent the extent to which fresh bedrock can be drained of the chemically equilibrated, nearly stagnant fluid that resides within it as it is uplifted. They propose that channel incision couples the evolution of surface topography with the evolution of the subsurface weathering profile by setting the pace of hillslope erosion and by mediating the slow drainage of fresh bedrock. In their model, the slope of the fresh bedrock surface depends, in part, on the saturated hydraulic conductivity of the fresh bedrock. Other bedrock weathering models point to the intrinsic differences in porosity of different rock types: Bazilevskaya et al. (2013), for example, interpreted an approximately tenfold deeper weathering front in granite compared to diabase to arise from significant fracturing and interconnected porosity in the granite, enabling the advection of oxygen to fresh mineral surfaces.

At Sagehorn (in the Central Belt), the hummocky topography indicates that earthflows were active in the past and extended from the ridge to the major channels (Dry and Hank). This ridge-to-channel slope creates a sustained head gradient in the underlying saturated fresh mélange but appears to have caused insignificant drainage in this dense, likely very low saturated conductivity material: The depth to fresh saturated bedrock at the divide is only a few meters. Frequent saturation overland flow results in localized surface erosion and the development of small valley networks that have cut into the stagnant earthflow features, creating a dense channel system bordered by convex hillslopes with a local relief of about 20 m (Figure 3 and supporting information Figure S6). Even these local ridges generate saturation overland flow in the winter, consistent with a shallow depth to fresh, low conductivity mélange, even in locally steeper areas.

We suggest that the mélange may represent an extreme end-member of low saturated conductivity, such that topographically driven head gradients are ineffective in causing drainage. Instead, given the shallow depths to fresh bedrock, water extraction—and thus weathering due to the introduction of oxygen and replacement of meteoric reactive water—may be driven only by transpiration and evaporation. In effect, the "bottom up" control is so strong—preventing deep lateral drainage—that the weathering front can only advance from these surface-driven processes. If so, the weathering front is strongly tied to the vegetation. The ~3-m depth to fresh bedrock in predominantly grassland areas may therefore reflect water extraction from previously widespread native perennial grasses, which have deeper roots than the present invasive annual grassland community (Dyer & Rice, 1999; Holmes & Rice, 1996).

Once drained, the Coastal Belt and Central Belt weather very differently. The shales of the Coastal Belt rapidly undergo slaking upon experiencing wetting and drying cycles, with rock disaggregating into millimeter- to centimeter-scale fragments once at the surface. This process is readily observable in previously saturated stream cobbles (supporting information Figure S7) as well as freshly incised bedrock channels and may, along with pyrite oxidation and mineral dissolution, create a network of fractures in the weathered rock zone that conveys water and holds a significant portion of the seasonally dynamic water storage. In contrast, augering observations and exposed stream cuts in the Central Belt suggest that weathered mélange matrix can deform in a manner that may tend to seal fractures, inhibiting the movement of water.

Together, these observations suggest that the distinct mineralogy and/or tectonic history between the Belts of the Franciscan result in different subsurface CZ structure in spite of similar bulk elemental composition, climate, and uplift history. The large differences in CZ structure have important ecohydrological consequences as they directly affect hillslope runoff pathways and seasonal water storage, and ultimately the composition and productivity of the ecosystems covering the landscape.

6. Conclusions

Adjacent plant communities and runoff patterns in the Northern California Coast Ranges vary strongly within a region of similar precipitation and temperature due to differences in the weathering of the underlying bedrock. Mixed broadleaf-needleleaf evergreen forests primarily inhabit the deeply weathered argillite and sandstones of the Coastal Belt, whereas a deciduous oak savanna-woodland with annual herbaceous ground cover inhabits the thinly weathered Central Belt mélange. Here we present direct evidence for lithologically controlled differences in bedrock weathering and water storage that explain these surface plant communities at regional (>100-km) scales. At our two field sites, we employ a unit hillslope approach in which we intensively monitored ecohydrologic processes on a hillslope within each rock type to explain ecological, runoff, and water budget differences observed at the catchment and regional scale. We find that subsurface dynamic water storage capacity scales with the depth of weathering. The Coastal Belt has a deep weathered zone—up to 30 m at ridgetops—and stores approximately 4 times more water seasonally than the Central Belt mélange, where fresh, unweathered parent material is found just ~2 to 4 m below the surface. Forests are sustained by the relatively high water content held at physiologically accessible water potentials within the hillslopes of the Coastal Belt. In the Central Belt mélange, less than 200 mm of precipitation leads to saturation of the subsurface, prompting widespread saturation overland flow and flashy stream runoff. This arises due to minimal water storage capacity and results in dry channel networks in the summer. Low water storage capacity results in low plant water availability and a community dominated by annual grasses and oaks that can extract tightly held water despite receiving ~1,800 mm of annual precipitation. A further factor likely limiting the establishment of the needleleaf tree *P. menziesii* (Douglas fir) is a seedling recruitment bottleneck due to the seasonal ground saturation. The differences in plant-available water availability between the two sites would not have been apparent from a study of the soils alone; the large differences in plant-available water storage capacity stem primarily from differences in the depth and extent of weathering in the bedrock underlying the soils.

Both sites are in areas of active uplift and channel incision, which will tend to drain the fresh bedrock and advance the weathering front. The underlying fresh Central Belt mélange bedrock, however, remains undrained (and unoxidized) even as channel incision drives hillslope evolution. This observation supports a "bottom-up" theory for control on depth to fresh bedrock. In the mélange, we propose that this control

is so strong that the drainage and advance of the weathering front (and corresponding development of porosity and water storage capacity) is accomplished by evaporation and transpiration withdrawal of moisture from the bedrock. In this seasonally dry Mediterranean climate, the extent to which the subsurface CZ sheds or stores precipitation during the wet season dictates dry season water availability and therefore the composition and productivity of ecosystems. Subsurface CZ water storage capacity regulation of plant water availability and community composition is likely widespread in seasonally dry climates. Deep drilling, intensive hydrologic monitoring on unit hillslopes, and catchment-wide storage analysis will help provide greater insight into the role of weathered bedrock in determining vegetation assemblages.

References

Aguiar, M. R., & Sala, O. E. (1994). Competition, facilitation, seed distribution and the origin of patches in a Patagonian Steppe. *Oikos*, *70*(1), 26–34. https://doi.org/10.2307/3545695

Allerup, P., & Madsen, H. (1980). Accuracy of point precipitation measurements. *Hydrology Research*, *11*(2), 57–70.

Amundson, R., Heimsath, A., Owen, J., Yoo, K., & Dietrich, W. E. (2015). Hillslope soils and vegetation. *Geomorphology*, *234*, 122–132. https://doi.org/10.1016/j.geomorph.2014.12.031

Anderson, M., Graham, R., Alyanakian, G., & Martynn, D. (1995). Late summer water status of soils and weathered bedrock in a Giant Sequoia grove. *Soil Science*, *160*(6), 415–422. https://doi.org/10.1097/00010694-199512000-00007

Anderson, M. G., & Ferree, C. E. (2010). Conserving the stage: Climate change and the geophysical underpinnings of species diversity. *PLoS ONE*, *5*(7), e11554. https://doi.org/10.1371/journal.pone.0011554

Anderson, R. S., Anderson, S. P., & Tucker, G. E. (2013). Rock damage and regolith transport by frost: an example of climate modulation of the geomorphology of the critical zone. *Earth Surface Processes and Landforms*, *38*(3), 299–316. https://doi.org/10.1002/esp.3330

Arkley, R. J. (1981). Soil moisture use by mixed conifer forest in a summer-dry climate. *Soil Science Society of America Journal*, *45*(2), 423–427. https://doi.org/10.2136/sssaj1981.03615995004500020037x

Armstrong, W. (1980). Aeration in higher plants. In H. W. Woolhouse (Ed.), *Advances in botanical research* (Vol. 7, pp. 225–332). London: Academic Press. https://doi.org/10.1016/S0065-2296(08)60089-0

Atwater, T., & Stock, J. (1998). Pacific-North America plate tectonics of the Neogene Southwestern United States: An update. *International Geology Review*, *40*(5), 375–402. https://doi.org/10.1080/00206819809465216

Bales, R. C., Hopmans, J. W., O'Geen, A. T., Meadows, M., Hartsough, P. C., Kirchner, P., et al. (2011). Soil moisture response to snowmelt and rainfall in a Sierra Nevada mixed-conifer forest. *Vadose Zone Journal*, *10*(3), 786. https://doi.org/10.2136/vzj2011.0001

Barkaoui, K., Navas, M.-L., Roumet, C., Cruz, P., & Volaire, F. (2017). Does water shortage generate water stress? An ecohydrological approach across Mediterranean plant communities. *Functional Ecology*, *31*(6), 1325–1335. https://doi.org/10.1111/1365-2435.12824

Bazilevskaya, E., Lebedeva, M., Pavich, M., Rother, G., Parkinson, D. Y., Cole, D., & Brantley, S. L. (2013). Where fast weathering creates thin regolith and slow weathering creates thick regolith. *Earth Surface Processes and Landforms*, *38*(8), 847–858. https://doi.org/10.1002/esp.3369

Bennett, G. L., Miller, S. R., Roering, J. J., & Schmidt, D. A. (2016). Landslides, threshold slopes, and the survival of relict terrain in the wake of the Mendocino Triple junction. *Geology*, *44*(5), 363–366. https://doi.org/10.1130/G37530.1

Bird, R. B., Bird, D. W., Codding, B. F., Parker, C. H., & Jones, J. H. (2008). The "fire stick farming" hypothesis: Australian Aboriginal foraging strategies, biodiversity, and anthropogenic fire mosaics. *Proceedings of the National Academy of Sciences of the United States of America*, *105*(39), 14,796–14,801. https://doi.org/10.1073/pnas.0804757105

Bish, D. L., & Howard, S. A. (1988). Quantitative phase analysis using the Rietveld method. *Journal of Applied Crystallography*, *21*(2), 86–91. https://doi.org/10.1107/S0021889887009415

Biswell, H. H. (1956). Ecology of California Grasslands. *Journal of Range Management*, *9*(1), 19–24. https://doi.org/10.2307/3894645

Blake, M. C., Jr, Jayko, A. S., & McLaughlin, R. J. (1985). Tectonostratigraphic terranes of the Northern Coast Ranges, California. Retrieved from http://archives.datapages.com/data/circ_pac/1/159_b.htm

Blake, M. C. B. (1974). Origin of Franciscan melanges in Northern California. Retrieved from http://archives.datapages.com/data/sepm_sp/SP19/Origin_of_Franciscan_Melanges_in_Northern_California.htm

Bond, W. J. (2005). Large parts of the world are brown or black: A different view on the 'Green World' hypothesis. *Journal of Vegetation Science*, *16*(3), 261–266. https://doi.org/10.1111/j.1654-1103.2005.tb02364.x

Boyer, J. S. (1995). *Measuring the water status of plants and soils*. New York: Academic Press, Inc. Retrieved from. http://udspace.udel.edu/handle/19716/2828

Branson, F., Miller, R., & McQueen, I. (1970). Plant communities and associated soil and water factors of shale-derived soil in Northeastern Montana. *Ecology*, *51*(3), 391–407. https://doi.org/10.2307/1935375

Burcham, L. T. (1957). *California range land: An historico-ecological study of the range resource of California*. Sacramento: Division of Forestry, Department of Natural Resources, State of California.

Clark, H. W. (1937). Association types in the North Coast Ranges of California. *Ecology*, *18*(2), 214–230. https://doi.org/10.2307/1930461d

Cloos, M. (1982). Flow melanges: Numerical modeling and geologic constraints on their origin in the Franciscan subduction complex, California. *Geological Society of America Bulletin*, *93*(4), 330–345. https://doi.org/10.1130/0016-7606(1982)93<330:FMNMAG>2.0.CO;2

Cloos, M. (1983). Comparative study of melange matrix and metashales from the Franciscan subduction complex with the Basal Great Valley Sequence, California. *The Journal of Geology*, *91*(3), 291–306.

Danielsen, K. C., & Halvorson, W. L. (1991). Valley oak seedling growth associated with selected grass species. In *Proceedings of the symposium on Oak Woodlands and Hardwood Rangeland Management, October 31–November 2, 1990* (Vol. 126, p. 9). Davis, CA: US Department of Agriculture, Pacific Southwest Research Station.

Dantas, V. d. L., Hirota, M., Oliveira, R. S., & Pausas, J. G. (2016). Disturbance maintains alternative biome states. *Ecology Letters*, *19*(1), 12–19. https://doi.org/10.1111/ele.12537

Davy, J. B. (1902). Stock ranges of Northwestern California, notes on the grasses and forage plants and range conditions. US Government Printing Office.

Dettinger, M. D., Ralph, F. M., Das, T., Neiman, P. J., & Cayan, D. R. (2011). Atmospheric rivers, floods and the water resources of California. *Water*, *3*(2), 445–478. https://doi.org/10.3390/w3020445

Dralle, D. N., Hahm, W. J., Rempe, D. M., Karst, N. J., Thompson, S. E., & Dietrich, W. E. (2018). Quantification of the seasonal hillslope water storage that does not drive streamflow. *Hydrological Processes*, *32*(13), 1978–1992.

Druhan, J. L., Fernandez, N., Wang, J., Dietrich, W. E., & Rempe, D. (2017). Seasonal shifts in the solute ion ratios of vadose zone rock moisture from the Eel River Critical Zone Observatory. *Acta Geochimica*, 1–4. https://doi.org/10.1007/s11631-017-0169-z

Dyer, A. R., & Rice, K. J. (1999). Effects of competition on resource availability and growth of a California bunchgrass. *Ecology*, *80*(8), 2697–2710. https://doi.org/10.1890/0012-9658(1999)080[2697:EOCORA]2.0.CO;2

Eliades, M., Bruggeman, A., Lubczynski, M. W., Christou, A., Camera, C., & Djuma, H. (2018). The water balance components of Mediterranean pine trees on a steep mountain slope during two hydrologically contrasting years. *Journal of Hydrology*, *562*, 712–724. https://doi.org/10.1016/j.jhydrol.2018.05.048

Ernst, W. G., & McLaughlin, R. J. (2012). Mineral parageneses, regional architecture, and tectonic evolution of Franciscan metagraywackes, Cape Mendocino-Garberville-Covelo 30′ × 60′ quadrangles, northwest California. *Tectonics*, *31*, TC1001. https://doi.org/10.1029/2011TC002987

Fellows, A. W., & Goulden, M. L. (2016). Mapping and understanding dry season soil water drawdown by California montane vegetation. *Ecohydrology*, *10*(1), e1772. https://doi.org/10.1002/eco.1772

Frenkel, R. E. (1977). *Ruderal vegetation along some California roadsides*. Berkeley: University of California Press.

Fuller, T. K., Perg, L. A., Willenbring, J. K., & Lepper, K. (2009). Field evidence for climate-driven changes in sediment supply leading to strath terrace formation. *Geology*, *37*(5), 467–470. https://doi.org/10.1130/G25487A.1

Gordon, D. R., Menke, J. M., & Rice, K. J. (1989). Competition for soil water between annual plants and blue oak (Quercus douglasii) seedlings. *Oecologia*, *79*(4), 533–541. https://doi.org/10.1007/BF00378672

Gordon, D. R., & Rice, K. J. (1993). Competitive effects of grassland annuals on soil water and Blue Oak (Quercus Douglasii) seedlings. *Ecology*, *74*(1), 68–82. https://doi.org/10.2307/1939502

Granger, D. E., Kirchner, J. W., & Finkel, R. (1996). Spatially averaged long-term erosion rates measured from in situ-produced cosmogenic nuclides in alluvial sediment. *The Journal of Geology*, *104*(3), 249–257. https://doi.org/10.1086/629823

Gromet, L. P., Haskin, L. A., Korotev, R. L., & Dymek, R. F. (1984). The "North American shale composite": Its compilation, major and trace element characteristics. *Geochimica et Cosmochimica Acta*, *48*(12), 2469–2482. https://doi.org/10.1016/0016-7037(84)90298-9

Gu, X., Rempe, D., & Brantley, S. L. (2016). Investigating the mechanisms of shale porosity development to understand hydrologic controls on hillslope scale weathering in a comparison across CZOs. In AGU Fall Meeting Abstracts. San Francisco, CA.

Hahm, W. J., Dietrich, W. E., & Dawson, T. E. (2017). Progressive depletion of stable isotopes recorded in a Mediterranean oak (Q. garryana) as a shallow saturated water source drains, leaving behind tightly held rock moisture. In Isotopes Switzerland 2017 Conference Proceedings. Mt. Verità, Ascona.

Hahm, W. J., Dietrich, W. E., & Dawson, T. E. (2018). Controls on the distribution and resilience of Q. garryana: Ecophysiological evidence of oak water-limitation tolerance. *Ecosphere*.

Hahm, W. J., Dralle, D. N., Lovill, S., Rose, J., Dawson, T. E., & Dietrich, W. E. (2017). Exploratory tree survey (2016—Eel River Critical Zone Observatory—Sagehorn—Central Belt Melange, Franciscan Complex, Northern California Coast Ranges, USA). *HydroShare*. https://doi.org/10.4211/hs.7881821a5c0e4ae3822b96a59f4bf8b6

Hahm, W. J., Rempe, D. M., & Dietrich, W. E. (2017). Direct measurements of seasonal groundwater and rock moisture storage in the deep Critical Zone reveal how lithology controls water availability and thus ecosystem characteristics in the Northern California Coast Ranges. In AGU-SEG Hydrogeophysics Workshop: Imaging the Critical Zone Abstracts. Stanford, CA.

Hahm, W. J., Riebe, C. S., Lukens, C. E., & Araki, S. (2014). Bedrock composition regulates mountain ecosystems and landscape evolution. *Proceedings of the National Academy of Sciences of the United States of America*, *111*(9), 3338–3343. https://doi.org/10.1073/pnas.1315667111

Hargreaves, G. H., & Samani, Z. A. (1982). Estimating potential evapotranspiration. *Journal of the Irrigation and Drainage Division*, *108*(3), 225–230.

Hargreaves, G. H., & Samani, Z. A. (1985). Reference crop evapotranspiration from temperature. *Applied Engineering in Agriculture*, *1*(2), 96–99. Retrieved from. https://elibrary.asabe.org/azdez.asp?AID=26773&t=2

Heilman, J. L., Litvak, M. E., McInnes, K. J., Kjelgaard, J. F., Kamps, R. H., & Schwinning, S. (2014). Water-storage capacity controls energy partitioning and water use in karst ecosystems on the Edwards Plateau, Texas. *Ecohydrology*, *7*(1), 127–138. https://doi.org/10.1002/eco.1327

Heinselman, M. L. (1981). Fire and succession in the conifer forests of Northern North America. In *Forest succession* (pp. 374–405). New York, NY: Springer. https://doi.org/10.1007/978-1-4612-5950-3_23

Hibbs, D. E., & Yoder, B. J. (1993). Development of Oregon white oak seedlings. *Northwest Science*, *67*(1), 30–36. Retrieved from https://research.wsulibs.wsu.edu:8443/xmlui/handle/2376/1570

Holdridge, L. R. (1947). Determination of world plant formations from simple climatic data. *Science*, *105*(2727), 367–368. https://doi.org/10.1126/science.105.2727.367

Holland, P. G., & Steyn, D. G. (1975). Vegetational responses to latitudinal variations in slope angle and aspect. *Journal of Biogeography*, *2*(3), 179–183. https://doi.org/10.2307/3037989

Holmes, T. H., & Rice, K. J. (1996). Patterns of growth and soil-water utilization in some exotic annuals and native perennial bunchgrasses of California. *Annals of Botany*, *78*(2), 233–243. https://doi.org/10.1006/anbo.1996.0117

Homer, C. G., Dewitz, J., Yang, L., Jin, S., Danielson, P., Xian, G., et al. (2015). Completion of the 2011 National Land Cover Database for the conterminous United States—Representing a decade of land cover change information. *Photogrammetric Engineering and Remote Sensing*, *81*(5), 345–354.

Huete, A., Didan, K., Miura, T., Rodriguez, E. P., Gao, X., & Ferreira, L. G. (2002). Overview of the radiometric and biophysical performance of the MODIS vegetation indices. *Remote Sensing of Environment*, *83*(1–2), 195–213. https://doi.org/10.1016/S0034-4257(02)00096-2

Huete, A. R., Didan, K., Shimabukuro, Y. E., Ratana, P., Saleska, S. R., Hutyra, L. R., et al. (2006). Amazon rainforests green-up with sunlight in dry season. *Geophysical Research Letters*, *33*, L06405. https://doi.org/10.1029/2005GL025583

Irwin, W. P. (1960). Geologic reconnaissance of the northern Coast Ranges and Klamath Mountains, California, with a summary of the mineral resources. San Francisco. Retrieved from http://archive.org/details/reconnaigeologic00irwirich

Jayko, A. S., Blake, M. C., McLaughlin, R. J., Ohlin, H. N., Ellen, S. D., & Kelsey, H. M. (1989). Reconnaissance geologic map of the Covelo 30- by 60-minute Quadrangle, Northern California (No. MF-2001). United States Geological Survey. Retrieved from http://ngmdb.usgs.gov/Prodesc/proddesc_327.htm

Johnson, S. (1979). The land-use history of the Coast Range Preserve, Mendocino County, California (MS). San Francisco State University.

Jones, D. P., & Graham, R. C. (1993). Water-holding characteristics of weathered granitic rock in chaparral and forest ecosystems. *Soil Science Society of America Journal*, *57*(1), 256–261. https://doi.org/10.2136/sssaj1993.03615995005700010044x

Kelly, A. E., & Goulden, M. L. (2008). Rapid shifts in plant distribution with recent climate change. *Proceedings of the National Academy of Sciences of the United States of America*, *105*, 11,823–11,826. https://doi.org/10.1073/pnas.0802891105

Kelsey, H. M. (1978). Earthflows in Franciscan melange, Van Duzen River basin, California. *Geology*, *6*(6), 361–364. https://doi.org/10.1130/0091-7613(1978)6<361:EIFMVD>2.0.CO;2

Kim, H., Bishop, J. K. B., Dietrich, W. E., & Fung, I. Y. (2014). Process dominance shift in solute chemistry as revealed by long-term high-frequency water chemistry observations of groundwater flowing through weathered argillite underlying a steep forested hillslope. *Geochimica et Cosmochimica Acta*, *140*, 1–19. https://doi.org/10.1016/j.gca.2014.05.011

Kim, H., Dietrich, W. E., Thurnhoffer, B. M., Bishop, J. K. B., & Fung, I. Y. (2017). Controls on solute concentration-discharge relationships revealed by simultaneous hydrochemistry observations of hillslope runoff and stream flow: The importance of critical zone structure. *Water Resources Research*, *53*, 1424–1443. https://doi.org/10.1002/2016WR019722

Klos, P. Z., Goulden, M. L., Riebe, C. S., Tague, C. L., O'Geen, A. T., Flinchum, B. A., et al. (2018). Subsurface plant-accessible water in mountain ecosystems with a Mediterranean climate. *Wiley Interdisciplinary Reviews Water*, *5*(3), e1277. https://doi.org/10.1002/wat2.1277

Kruckeberg, A. R. (1985). *California serpentines: Flora, vegetation, geology, soils, and management problems*. Berkeley: University of California Press.

Kruckeberg, A. R. (2004). *Geology and plant life: The effects of landforms and rock types on plants*. Seattle, WA: University of Washington Press.

Krygier, J. T. (1971). Project completion report on comparative water loss of Douglas-fir and Oregon white oak: Part of the study of hydrology of water yield prediction. Water Resources Research Institute and School of Forestry, Oregon State University.

Laio, F., Porporato, A., Ridolfi, L., & Rodriguez-Iturbe, I. (2001). Plants in water-controlled ecosystems: active role in hydrologic processes and response to water stress: II. Probabilistic soil moisture dynamics. *Advances in Water Resources*, *24*(7), 707–723. https://doi.org/10.1016/S0309-1708(01)00005-7

Langenheim, V. E., Jachens, R. C., Wentworth, C. M., & McLaughlin, R. J. (2013). Previously unrecognized regional structure of the Coastal Belt of the Franciscan Complex, northern California, revealed by magnetic data. *Geosphere*, *9*(6), 1514–1529. https://doi.org/10.1130/GES00942.1

Lebedeva, M. I., & Brantley, S. L. (2013). Exploring geochemical controls on weathering and erosion of convex hillslopes: Beyond the empirical regolith production function. *Earth Surface Processes and Landforms*, *38*(15), 1793–1807. https://doi.org/10.1002/esp.3424

Lewis, D. C., & Burgy, R. H. (1964). The relationship between oak tree roots and groundwater in fractured rock as determined by tritium tracing. *Journal of Geophysical Research*, *69*(12), 2579–2588. https://doi.org/10.1029/JZ069i012p02579

Lightfoot, K. G., & Parrish, O. (2009). *California Indians and their environment: An introduction*. Berkeley, CA: University of California Press.

Link, P., Simonin, K., Maness, H., Oshun, J., Dawson, T., & Fung, I. (2014). Species differences in the seasonality of evergreen tree transpiration in a Mediterranean climate: Analysis of multiyear, half-hourly sap flow observations. *Water Resources Research*, *50*, 1869–1894. https://doi.org/10.1002/2013WR014023

Lock, J., Kelsey, H., Furlong, K., & Woolace, A. (2006). Late Neogene and quaternary landscape evolution of the northern California Coast Ranges: Evidence for Mendocino triple junction tectonics. *Geological Society of America Bulletin*, *118*(9–10), 1232–1246. https://doi.org/10.1130/B25885.1

Lovill, S., Hahm, W. J., & Dietrich, W. E. (2018). Drainage from the critical zone: Lithologic controls on the persistence and spatial extent of wetted channels during the summer dry season. *Water Resources Research*, *54*, 5702–5726. https://doi.org/10.1029/2017WR021903

Mackey, B. H., & Roering, J. J. (2011). Sediment yield, spatial characteristics, and the long-term evolution of active earthflows determined from airborne LiDAR and historical aerial photographs, Eel River, California. *Geological Society of America Bulletin*, *123*(7–8), 1560–1576. https://doi.org/10.1130/B30306.1

Martin, R. E., & Sapis, D. B. (1991). Fires as agents of biodiversity: Pyrodiversity promotes biodiversity. In *Proceedings of the symposium on biodiversity of Northwestern California* (pp. 150–157). Santa Rosa, CA: Cooperative Extension, University of California, Berkeley.

McDonnell, J. J., Evaristo, J., Bladon, K. D., Buttle, J., Creed, I. F., Dymond, S. F., et al. (2018). Water sustainability and watershed storage. *Nature Sustainability*, *1*(8), 378–379. https://doi.org/10.1038/s41893-018-0099-8

McLaughlin, R. J., Sliter, W. V., Frederiksen, N. O., Harbert, W. P., & McCulloch, D. S. (1994). Plate motions recorded in tectonostratigraphic terranes of the Franciscan Complex and evolution of the Mendocino triple junction, northwestern California (no. 1997). USGS. Retrieved from. https://pubs.er.usgs.gov/publication/b1997

McNamara, J. P., Tetzlaff, D., Bishop, K., Soulsby, C., Seyfried, M., Peters, N. E., et al. (2011). Storage as a metric of catchment comparison. *Hydrological Processes*, *25*(21), 3364–3371. https://doi.org/10.1002/hyp.8113

Mensing, S. (2006). The history of oak woodlands in California, part II: The native American and historic period. *The California Geographer*, *46*(5), 1–31. Retrieved from. http://scholarworks.calstate.edu/handle/10211.2/2770

Miller, G. R., Chen, X., Rubin, Y., Ma, S., & Baldocchi, D. D. (2010). Groundwater uptake by woody vegetation in a semiarid oak savanna. *Water Resources Research*, *46*, W10503. https://doi.org/10.1029/2009WR008902

Milly, P. C. D. (1994). Climate, interseasonal storage of soil water, and the annual water balance. *Advances in Water Resources*, *17*(1), 19–24. https://doi.org/10.1016/0309-1708(94)90020-5

Milly, P. C. D., & Dunne, K. A. (1994). Sensitivity of the global water cycle to the water-holding capacity of land. *Journal of Climate*, *7*(4), 506–526. https://doi.org/10.1175/1520-0442(1994)007<0506:SOTGWC>2.0.CO;2

Minore, D. (1968). Effects of artificial flooding on seedling survival and growth of six northwestern tree species. Retrieved from http://agris.fao.org/agris-search/search.do?recordID=US201300321958

Miralles, D. G., Gash, J. H., Holmes, T. R. H., de Jeu, R. A. M., & Dolman, A. J. (2010). Global canopy interception from satellite observations. *Journal of Geophysical Research*, *115*, D16122. https://doi.org/10.1029/2009JD013530

Oshun, J., Dietrich, W. E., Dawson, T. E., & Fung, I. (2016). Dynamic, structured heterogeneity of water isotopes inside hillslopes. *Water Resources Research*, *52*, 164–189. https://doi.org/10.1002/2015WR017485

Parker, A. J. (1982). The topographic relative moisture index: An approach to soil-moisture assessment in mountain terrain. *Physical Geography*, *3*(2), 160–168. https://doi.org/10.1080/02723646.1982.10642224

Pfister, L., Martínez-Carreras, N., Hissler, C., Klaus, J., Carrer, G. E., Stewart, M. K., & McDonnell, J. J. (2017). Bedrock geology controls on catchment storage, mixing, and release: A comparative analysis of 16 nested catchments. *Hydrological Processes*, *31*(10), 1828–1845. https://doi.org/10.1002/hyp.11134

Polis, G. A. (1999). Why are parts of the world green? Multiple factors control productivity and the distribution of biomass. *Oikos*, *86*(1), 3–15. https://doi.org/10.2307/3546565

Popenoe, J. H., Bevis, K. A., Gordon, B. R., Sturhan, N. K., & Hauxwell, D. L. (1992). Soil-vegetation relationships in Franciscan terrain of northwestern California. *Soil Science Society of America Journal*, *56*(6), 1951–1959. https://doi.org/10.2136/sssaj1992.03615995005600060050x

Porporato, A., Daly, E., & Rodriguez-Iturbe, I. (2004). Soil water balance and ecosystem response to climate change. *The American Naturalist*, *164*(5), 625–632. https://doi.org/10.1086/424970

Porporato, A., Laio, F., Ridolfi, L., & Rodriguez-Iturbe, I. (2001). Plants in water-controlled ecosystems: Active role in hydrologic processes and response to water stress. *Advances in Water Resources*, *24*(7), 725–744. https://doi.org/10.1016/S0309-1708(01)00006-9

Prentice, I. C., Cramer, W., Harrison, S. P., Leemans, R., Monserud, R. A., & Solomon, A. M. (1992). Special paper: A global biome model based on plant physiology and dominance, soil properties and climate. *Journal of Biogeography*, *19*(2), 117–134. https://doi.org/10.2307/2845499

Pypker, T. G., Bond, B. J., Link, T. E., Marks, D., & Unsworth, M. H. (2005). The importance of canopy structure in controlling the interception loss of rainfall: Examples from a young and an old-growth Douglas-fir forest. *Agricultural and Forest Meteorology*, *130*(1), 113–129. https://doi.org/10.1016/j.agrformet.2005.03.003

Rantz, S. E. (1968). Average annual precipitation and runoff in north coastal California (USGS Numbered Series No. 298). Retrieved from http://pubs.er.usgs.gov/publication/ha298

Reid, L. M., & Lewis, J. (2009). Rates, timing, and mechanisms of rainfall interception loss in a coastal redwood forest. *Journal of Hydrology*, *375*(3–4), 459–470. https://doi.org/10.1016/j.jhydrol.2009.06.048

Rempe, D. M., & Dietrich, W. E. (2014). A bottom-up control on fresh-bedrock topography under landscapes. *Proceedings of the National Academy of Sciences of the United States of America*, *111*(18), 6576–6581. https://doi.org/10.1073/pnas.1404763111

Rempe, D. M., & Dietrich, W. E. (2018). Direct observations of rock moisture, a hidden component of the hydrologic cycle. *Proceedings of the National Academy of Sciences of the United States of America*, *115*(11), 2664–2669.

Ricklefs, R. E. (2008). *The Economy of Nature*. Macmillan, New York: W.H. Freeman.

Riebe, C. S., Hahm, W. J., & Brantley, S. L. (2017). Controls on deep critical zone architecture: A historical review and four testable hypotheses. *Earth Surface Processes and Landforms*, *42*(1), 128–156. https://doi.org/10.1002/esp.4052

Rittiman, C., & Thorson, T. (2001). Soil survey of Mendocino County. California, Western Part, Mendocino County Resource Conservation District.

Robinson, N. P., Allred, B. W., Smith, W. K., Jones, M. O., Moreno, A., Erickson, T. A., et al. (2018). Terrestrial primary production for the conterminous United States derived from Landsat 30 m and MODIS 250 m. *Remote Sensing in Ecology and Conservation*, *4*(3), 264–280. https://doi.org/10.1002/rse2.74

Rodriguez-Iturbe, I., D'Odorico, P., Laio, F., Ridolfi, L., & Tamea, S. (2007). Challenges in humid land ecohydrology: Interactions of water table and unsaturated zone with climate, soil, and vegetation. *Water Resources Research*, *43*, W09301. https://doi.org/10.1029/2007WR006073

Roering, J. J., Mackey, B. H., Handwerger, A. L., Booth, A. M., Schmidt, D. A., Bennett, G. L., & Cerovski-Darriau, C. (2015). Beyond the angle of repose: A review and synthesis of landslide processes in response to rapid uplift, Eel River, Northern California. *Geomorphology*, *236*, 109–131. https://doi.org/10.1016/j.geomorph.2015.02.013

Roering, J. J., Stimely, L. L., Mackey, B. H., & Schmidt, D. A. (2009). Using DInSAR, airborne LiDAR, and archival air photos to quantify landsliding and sediment transport. *Geophysical Research Letters*, *36*, L19402. https://doi.org/10.1029/2009GL040374

Rose, K., Graham, R., & Parker, D. (2003). Water source utilization by Pinus jeffreyi and Arctostaphylos patula on thin soils over bedrock. *Oecologia*, *134*(1), 46–54. https://doi.org/10.1007/s00442-002-1084-4

Rouholahnejad Freund, E., & Kirchner, J. W. (2017). A Budyko framework for estimating how spatial heterogeneity and lateral moisture redistribution affect average evapotranspiration rates as seen from the atmosphere. *Hydrology and Earth System Sciences*, *21*(1), 217–233. https://doi.org/10.5194/hess-21-217-2017

Ryu, Y., Baldocchi, D. D., Kobayashi, H., van Ingen, C., Li, J., Black, T. A., et al. (2011). Integration of MODIS land and atmosphere products with a coupled-process model to estimate gross primary productivity and evapotranspiration from 1 km to global scales. *Global Biogeochemical Cycles*, *25*, GB4017. https://doi.org/10.1029/2011GB004053

Salve, R., Rempe, D. M., & Dietrich, W. E. (2012). Rain, rock moisture dynamics, and the rapid response of perched groundwater in weathered, fractured argillite underlying a steep hillslope. *Water Resources Research*, *48*, W11528. https://doi.org/10.1029/2012WR012583

Sayama, T., McDonnell, J. J., Dhakal, A., & Sullivan, K. (2011). How much water can a watershed store? *Hydrological Processes*, *25*(25), 3899–3908. https://doi.org/10.1002/hyp.8288

Scanlon, T. M., Caylor, K. K., Levin, S. A., & Rodriguez-Iturbe, I. (2007). Positive feedbacks promote power-law clustering of Kalahari vegetation. *Nature*, *449*(7159), 209–212. https://doi.org/10.1038/nature06060

Schieber, J. (2010). Common themes in the formation and preservation of intrinsic porosity in shales and mudstones—Illustrated with examples across the Phanerozoic. Presented at the SPE Unconventional Gas Conference, Society of Petroleum Engineers. https://doi.org/10.2118/132370-MS

Scholander, P. F., Bradstreet, E. D., Hemmingsen, E. A., & Hammel, H. T. (1965). Sap pressure in vascular plants: Negative hydrostatic pressure can be measured in plants. *Science*, *148*(3668), 339–346. https://doi.org/10.1126/science.148.3668.339

Schriver, M., Sherriff, R. L., Varner, J. M., Quinn-Davidson, L., & Valachovic, Y. (2018). Age and stand structure of oak woodlands along a gradient of conifer encroachment in northwestern California. *Ecosphere*, *9*(10), e02446. https://doi.org/10.1002/ecs2.2446

Schwinning, S. (2010). The ecohydrology of roots in rocks. *Ecohydrology*, *3*(2), 238–245. https://doi.org/10.1002/eco.134

Seidl, M., & Dietrich, W. E. (1992). The problem of channel erosion into bedrock. In *Catena supplement* (Vol. 23, pp. 101–124). Cremlingen: Verlag.

Sevruk, B. (1982). Methods of correction for systematic error in point precipitation measurement for operational use. Secretariat of the World Meteorological Organization.

Simonin, K. A., Link, P., Rempe, D., Miller, S., Oshun, J., Bode, C., et al. (2014). Vegetation induced changes in the stable isotope composition of near surface humidity. *Ecohydrology*, *7*(3), 936–949. https://doi.org/10.1002/eco.1420

Smith, S. D., Herr, C. A., Leary, K. L., & Piorkowski, J. M. (1995). Soil-plant water relations in a Mojave Desert mixed shrub community: A comparison of three geomorphic surfaces. *Journal of Arid Environments*, *29*(3), 339–351. https://doi.org/10.1016/S0140-1963(05)80113-2

Smith, T. J., McNamara, J. P., Flores, A. N., Gribb, M. M., Aishlin, P. S., & Benner, S. G. (2011). Small soil storage capacity limits benefit of winter snowpack to upland vegetation. *Hydrological Processes*, *25*(25), 3858–3865. https://doi.org/10.1002/hyp.8340

St. Clair, J., Moon, S., Holbrook, W. S., Perron, J. T., Riebe, C. S., Martel, S. J., et al. (2015). Geophysical imaging reveals topographic stress control of bedrock weathering. *Science*, *350*(6260), 534–538. https://doi.org/10.1126/science.aab2210

Stein, W. (1990). Quercus garryana Dougl. ex hook. Oregon white oak. In R. M. Burns, B. H. Honkala, & Tech. Coords (Eds.), *Silvics of North America, volume II: Hardwoods* (Vol. 2, pp. 650–660). Washington, DC: USDA Forest Service.

Stephenson, N. L. (1990). Climatic control of vegetation distribution: The role of the water balance. *The American Naturalist*, *135*(5), 649–670. https://doi.org/10.2307/2462028

Sternberg, P. D., Anderson, M. A., Graham, R. C., Beyers, J. L., & Tice, K. R. (1996). Root distribution and seasonal water status in weathered granitic bedrock under chaparral. *Geoderma*, *72*, 89–98.

Stock, G. M., Anderson, R. S., & Finkel, R. C. (2005). Rates of erosion and topographic evolution of the Sierra Nevada, California, inferred from cosmogenic 26Al and 10Be concentrations. *Earth Surface Processes and Landforms*, *30*(8), 985–1006. https://doi.org/10.1002/esp.1258

Stone, J. O. (2000). Air pressure and cosmogenic isotope production. *Journal of Geophysical Research*, *105*(B10), 23,753–23,759. https://doi.org/10.1029/2000JB900181

Syvitski, J. P., & Morehead, M. D. (1999). Estimating river-sediment discharge to the ocean: Application to the Eel margin, northern California. *Marine Geology*, *154*(1–4), 13–28. https://doi.org/10.1016/S0025-3227(98)00100-5

Tetzlaff, D., McNamara, J. P., & Carey, S. K. (2011). Measurements and modelling of storage dynamics across scales. *Hydrological Processes*, *25*(25), 3831–3835. https://doi.org/10.1002/hyp.8396

Trauernicht, C., Brook, B. W., Murphy, B. P., Williamson, G. J., & Bowman, D. M. J. S. (2015). Local and global pyrogeographic evidence that indigenous fire management creates pyrodiversity. *Ecology and Evolution*, *5*(9), 1908–1918. https://doi.org/10.1002/ece3.1494

Vermeesch, P. (2007). CosmoCalc: An Excel add-in for cosmogenic nuclide calculations. *Geochemistry, Geophysics, Geosystems*, *8*, Q08003. https://doi.org/10.1029/2006GC001530

Whittaker, R. H. (1975). *Communities and ecosystems* (2nd ed.). New York: Macmillan Company. Retrieved from http://repositories.tdl.org/tamug-ir/handle/1969.3/27436

Yang, D., Goodison, B. E., Metcalfe, J. R., Golubev, V. S., Bates, R., Pangburn, T., & Hanson, C. L. (1998). Accuracy of NWS 8? Standard nonrecording precipitation gauge: Results and application of WMO Intercomparison. *Journal of Atmospheric and Oceanic Technology*, *15*(1), 54–68. https://doi.org/10.1175/1520-0426(1998)015<0054:AONSNP>2.0.CO;2

Yang, H., Yang, D., Lei, Z., & Sun, F. (2008). New analytical derivation of the mean annual water-energy balance equation. *Water Resources Research*, *44*, W03410. https://doi.org/10.1029/2007WR006135

Zaerr, J. B. (1983). Short-term flooding and net photosynthesis in seedlings of three conifers. *Forest Science*, *29*(1), 71–78.

Zunzunegui, M., Boutaleb, S., Díaz Barradas, M. C., Esquivias, M. P., Valera, J., Jáuregui, J., et al. (2018). Reliance on deep soil water in the tree species Argania spinosa. *Tree Physiology*, *38*(5), 678–689. https://doi.org/10.1093/treephys/tpx152

Zwieniecki, M. A., & Newton, M. (1996). Seasonal pattern of water depletion from soil–rock profiles in a Mediterranean climate in southwestern Oregon. *Canadian Journal of Forest Research*, *26*(8), 1346–1352. https://doi.org/10.1139/x26-150